

The projection method for the incompressible Navier-Stokes equations: The pressure near a no-slip wall

A.W. Vreman

AkzoNobel, Research Development & Innovation, Process Technology, P.O. Box 10, 7400 AA Deventer, The Netherlands

Preprint of a paper published in Journal of Computational Physics 263, 353-374 (2014)

Abstract

An explicit staggered projection method for the incompressible Navier-Stokes equations with no-slip walls is analyzed and used in simulations to address several issues related to the pressure boundary condition required when the continuity equation is replaced by the standard pressure Poisson equation (PPE), $\nabla^2 p = \nabla \cdot (-\mathbf{u} \cdot \nabla \mathbf{u} + \mathbf{f})$. First, it is shown that a PPE system supplemented with a Neumann pressure boundary condition derived from the momentum equation can be made consistent with the Navier-Stokes equations if it is extended with the requirement that $\nabla \cdot \nabla^2 \mathbf{u} = 0$ is zero near the wall and the solution is sufficiently smooth. This implies that it is possible to formulate a boundary condition for the standard PPE without the necessity to resort to Green's functions, which is interesting for theoretical reasons. Second, the equivalence is shown between the staggered projection method and the staggered discretization of above PPE system. The derivation of the equivalence sheds light upon the so-called PPE paradox and leads to an approximation of the wall value of $\partial p / \partial n$, which is not required but implied by the staggered projection method. Third, the (near-wall) regularity of a solution of the Navier-Stokes equations is numerically analyzed by means of Direct Numerical Simulation of turbulent channel flow performed with the staggered projection method. From the numerical inspection of all terms of the momentum equation in the near-wall region, it is concluded that the three components of the momentum equation are satisfied on the wall for $t > 0$ (for short times, but also in the turbulent regime). In the limit $t \rightarrow 0$, the pressure gradient is observed to converge to the initial pressure gradient in the L_2 -norm, which confirms a disputed theoretical result in literature. Even in the maximum norm, the pressure gradient appears to converge to the initial pressure gradient. The only discontinuities observed in the simulations are the discontinuities of the tangential viscous terms and the time derivatives of the tangential velocities on the wall at $t = 0$. Thus the numerical results indicate that the regularity of the solution for turbulent channel flow is stronger than claimed by existing theory.

Keywords: projection method, staggered methods, Navier-Stokes equations, pressure Poisson equation, pressure boundary condition, DNS of turbulent channel flow

1. Introduction

The behaviour of the pressure near a no-slip wall and in particular the appropriate wall boundary condition for the pressure Poisson equation deduced from the Navier-Stokes equations have been widely discussed in literature [1, 2, 3, 4, 5, 6, 7, 8, 9]. The literature on these topics easily causes confusion; contradicting statements, claims and even contradicting theorems can be found. In the present paper these issues are reconsidered and interpreted with use of Direct Numerical Simulation (DNS) of turbulent channel flow.

Before we mention the aims and approach of the present paper in more detail, we specify the Navier-Stokes equations and mention several pressure Poisson equations that can be found in literature. We also recapitulate some relevant theoretical results on the regularity of solutions for the Navier-Stokes equations in a wall-bounded domain.

Email address: bert.vreman@akzonobel.com, bert@vremanresearch.nl (A.W. Vreman)

The Navier-Stokes equations are formulated for incompressible plane channel flow in the spatial domain $\Omega = [0, L_x] \times (0, L_y) \times [0, L_z]$ for time $t \geq 0$. The two parallel walls are given by $\Gamma = [0, L_x] \times \{0, L_y\} \times [0, L_z]$, such that $\bar{\Omega} = \Omega \cup \Gamma$. Pressure and velocity are denoted by p and $\mathbf{u} = (u, v, w)$, respectively, and depend on location $\mathbf{x} = (x, y, z)$ and t . The pressure is defined as a function with a volume integral of zero. In streamwise direction (x) and spanwise direction (z), periodic boundary conditions are imposed on p and \mathbf{u} . In the normal direction, no-slip boundary conditions are imposed to the velocity. The velocity prescribed on Γ is denoted by \mathbf{u}_Γ . The Navier-Stokes equations for incompressible flow in the space-time domain $\Omega \times (0, \infty)$ read:

$$\nabla \cdot \mathbf{u} = 0, \quad (1)$$

$$\partial \mathbf{u} / \partial t = -\mathbf{u} \cdot \nabla \mathbf{u} - \nabla p + \nu \nabla^2 \mathbf{u} + \mathbf{f}, \quad (2)$$

$$\mathbf{u} = \mathbf{u}_\Gamma \text{ on } \Gamma; \quad \mathbf{u}, p \text{ periodic in } x, z; \quad \int_{\Omega} p dV = 0; \quad \mathbf{u}(\mathbf{x}, 0) = \mathbf{u}^0(\mathbf{x}). \quad (3)$$

Here ν is the kinematic viscosity, $\mathbf{f}(\mathbf{x}, t)$ a smooth (C^∞) forcing term, and $\mathbf{u}^0(\mathbf{x})$ a smooth initial velocity field with $\nabla \cdot \mathbf{u}^0 = 0$ in Ω and $\mathbf{u}^0(\mathbf{x}) = \mathbf{u}_\Gamma(\mathbf{x}, 0)$ for $\mathbf{x} \in \Gamma$. The velocity $\mathbf{u}_\Gamma(\mathbf{x}, t)$ is defined as a smooth vector field on Γ that satisfies the periodic boundary conditions in x and z . The normal velocity on the wall, v_Γ , is a function with the property that its integral over Γ is zero. For the time being the local value of \mathbf{u}_Γ is not assumed to be zero, to generalize the formulation to sliding walls, nonpermeable walls or velocity specified inflow boundary conditions. Equations (1-3) are frequently called the primitive equations, we will refer to these equations as system NS. It is stressed that in system NS no boundary condition for the pressure on Γ is specified.

Application of the divergence to Eq. (2) and $\partial/\partial t$ to Eq. (1) provides the standard pressure Poisson equation (PPE)

$$\nabla^2 p = \nabla \cdot (-\mathbf{u} \cdot \nabla \mathbf{u} + \mathbf{f}). \quad (4)$$

With the differentiation the order of the equation has increased and therefore a boundary condition for the pressure is required to solve Eq. (4). One procedure to obtain the required boundary condition is the matrix influence method proposed by Kleiser and Schumann [2] in the context of spectral methods. With the use of Green's functions, this method provides a Dirichlet boundary condition for p on Γ by imposing $\nabla \cdot \mathbf{u} = 0$ on Γ at the new time level. The system of equations (1-4) equipped with the matrix influence Dirichlet boundary condition for p will be called PPE0. The implementation of PPE0 is complicated.

A simpler procedure to specify a wall boundary condition for the pressure Poisson equation is the derivation of a Neumann pressure boundary condition from the momentum equation in the normal direction. This procedure is used in system PPE1 [5], defined by (2-4) and

$$\frac{\partial p}{\partial y} = \nu \nabla^2 v + f_y - \mathbf{u}_\Gamma \cdot \nabla v - \frac{\partial v_\Gamma}{\partial t} \quad \text{on } \Gamma. \quad (5)$$

The last two terms vanish if $\mathbf{u}_\Gamma = \mathbf{0}$, and also if \mathbf{u}_Γ does not depend on time and $\nabla \cdot \mathbf{u} = 0$ on Γ (since then $\nabla v = 0$ on Γ). Gresho and Sani [5] discussed PPE1 in detail and formulated an hypothesis that NS and PPE1 would be equivalent. However, this hypothesis was falsified by the same authors in later work [7] and [9]; an example in section 3.10.3 of Ref. [7] shows that PPE1 is ill-posed.

Gresho and Sani [5] also introduced system PPE2, defined by (2-3), Poisson equation

$$\nabla^2 p = \nabla \cdot (-\mathbf{u} \cdot \nabla \mathbf{u} + \nu \nabla^2 \mathbf{u} + \mathbf{f}), \quad (6)$$

and boundary condition (5). The so-called PPE paradox "if you include it, you do not need it, but if you do not include it, you do need it" [7] refers to the inclusion of the term $\nu \nabla \cdot \nabla^2 \mathbf{u}$, which is zero, into the right-hand side of this Poisson equation. The standard Poisson equation (4) is also called the simplified Poisson equation [5], while (6) is also called the consistent Poisson equation.

In the derivation of a pressure boundary condition from the momentum equation it is not obvious why the momentum equation in the normal direction should be chosen and whether the choice of one of the other momentum equations would imply a different solution. This ambiguity was pointed out in several papers, see for example [1, 4], and led to a theorem with a corollary that PPE2 would be ill-posed [8], but according to Ref. [9] this statement is incorrect.

The discussion in literature about the PPE1 and PPE2 prompts research question I: *Is there another way to extend PPE1 such that it becomes consistent, without the term $\nu \nabla \cdot \nabla^2 \mathbf{u}$ in the Poisson equation, but with the Neumann boundary condition?* In answer to this question a new PPE system is proposed, PPE3, which consists of equations (2-5) and the additional near-wall requirement

$$\nabla \cdot \nabla^2 \mathbf{u} = 0 \quad \text{in the neighbourhood of } \Gamma, \quad (7)$$

i.e. the divergence of the Laplacian of the velocity should be zero for $\mathbf{x} \in \Omega$ infinitesimally close to Γ . Thus system PPE3 is essentially PPE1 extended with condition (7).

The difficult and confusing part of PPE systems is related to the pressure boundary condition of the PPE at the wall. We are therefore interested in the behaviour of the pressure gradient near a no-slip wall. For a numerical investigation of the behaviour of the pressure gradient near the wall, it is convenient to use a pressure-based method which does not require a boundary condition for the pressure on Γ . The Marker and Cell (MAC) method introduced by Harlow and Welch [10] is such a method, since it is a direct discretization of system NS (1-3), on a staggered grid. Another well-known method to solve system NS is the projection method, introduced by Chorin [11] and Temam [12]. In case of explicit treatment of the convective and implicit treatment of the viscous terms, which introduces a splitting error, the projection method is also called the fractional step method [1, 13]. The projection of an intermediate velocity on the space of divergence free functions leads to an implicit equation for the pressure. On a staggered grid and entirely formulated in discrete space the definition of a pressure boundary condition can be avoided [13], such that, like the MAC method, the projection method can also be regarded as a direct discretization of system NS [3, 6, 13, 14]. The formulation of the projection method on staggered grids in discrete space is appealing, but it is still unclear how we should interpret the circumvention of the pressure boundary condition, since the discrete implicit equation is very similar to a discretized Poisson equation for the pressure. This prompts research question II: *Which continuous pressure Poisson equation problem leads to the standard staggered projection method, that apparently does not require a pressure boundary condition?*

In the answers to this and the first research question, PPE3 plays a central role. System PPE3 is not introduced for computational efficiency but for theoretical purposes, such as the clarification of the connection between PPE systems and the projection method, the clarification of the PPE paradox, and the derivation of the wall value of $\partial p / \partial n$ implied by the projection method. An appealing theoretical feature of PPE3 is that it is just the standard Poisson equation supplemented with the Neumann pressure boundary condition and a simple additional condition that can be implemented without a matrix influence method and Green's functions.

If the pressure boundary condition for a pressure Poisson equation is based on a component of the momentum equation, like in Eq. (5), it is important that the terms used in that component of the momentum equation are continuous in the near-wall limit. A quantity is called discontinuous in the near-wall limit if the space-time limit approaching some point on the wall does not exist. Possible discontinuities in the tangential directions are an important reason to derive the boundary condition from the normal component momentum equation and not from the tangential ones; in Refs. [5, 7] the use of the normal component has been justified with reference to an analytical result in Heywood and Rannacher [16], but unfortunately precisely this result is contradicted in later literature by another analytical argument [8], as will be explained later on. For these reasons we will numerically explore the regularity of a solution of the Navier-Stokes equation with a focus on the near-wall behaviour of the pressure gradient and other terms in the momentum equation.

The main reason of the problems and contradictions in literature on PPE systems seems to be that, despite the smooth initial condition, the solution of NS for wall-bounded flows is not necessarily smooth. Problems particularly arise in the limit $t \rightarrow 0$, since the initial condition does not necessarily satisfy the compatibility conditions that follow from the requirement of infinite differentiability in space and time of the solution on Γ at $t = 0$ [15, 16]. To specify a divergence free initial condition \mathbf{u}^0 that satisfies the compatibility conditions seems desirable, but this appears to be very difficult. Consider for example the conditions that would arise if we would require continuous $\partial \mathbf{u} / \partial t$ on Γ , which can be expressed as three boundary conditions for the initial pressure p^0 :

$$\nabla p^0 = \nu \nabla^2 \mathbf{u}^0 + \mathbf{f}^0 - \mathbf{u}^0 \cdot \nabla \mathbf{u}^0 - \frac{\partial \mathbf{u}_\Gamma}{\partial t}(\mathbf{x}, 0) \quad \text{on } \Gamma, \quad (8)$$

in combination with $\nabla^2 p^0 = \nabla \cdot (-\mathbf{u}^0 \cdot \nabla \mathbf{u}^0 + \mathbf{f}^0)$, where $\mathbf{f}^0 = \mathbf{f}(\mathbf{x}, 0)$. To find a divergence-free \mathbf{u}^0 , such that a p^0 exists that satisfies above three boundary conditions and the Poisson equation, is far from trivial.

At this point we rephrase two theoretical regularity results for system NS:

- H1980 (Heywood [15]; Theorem 9, see also [17]). There exists a classical solution (\mathbf{u}, p) of problem NS on some time interval $(0, T)$, such that (a) \mathbf{u} is smooth (C^∞) on $\Omega \times (0, T)$, (b) \mathbf{u} is continuous on $\bar{\Omega} \times [0, T)$ (so also at $t = 0$ and at the wall Γ), and (c) the first- and higher-order time derivatives of \mathbf{u} are continuous on $\bar{\Omega} \times (0, T)$ (so also on Γ , but not necessarily at $t = 0$).
- HR1982 (Heywood & Rannacher [16]; Proposition 2.1). Define the pressure p^0 as the solution of the (generalized) Poisson equation in system PPE1 at $t = 0$. The solution p^0 exists, is unique up to a constant, and is continuously differentiable on Ω . A classical solution \mathbf{u}, p of NS satisfies

$$\|\nabla p - \nabla p^0\|_2 \rightarrow 0 \quad \text{if} \quad t \rightarrow 0, \quad (9)$$

where $\|\cdot\|_2$ denotes the L_2 -norm on Ω .

The first result (H1980) is important, but it does not state that the existing solution is unique nor that it exists for infinite time. Apparently, HR1980 does not rule out ill-posedness of system NS. The second result (HR1982), which has been used to justify PPE systems with a Neumann boundary condition [5], is controversial, in the sense that Lemma 3 in Ref. [8] claims the opposite, namely that the pressure gradient is discontinuous at $t = 0$ ($\lim_{t \rightarrow 0} \|\nabla p - \nabla p^0\|_2 > 0$).

Reflecting on what is theoretically known about the initial boundary value problem of the Navier-Stokes equations in wall-bounded domains and the apparent confusion this problem has caused, one may wonder whether Direct Numerical Simulation (DNS) of wall-bounded incompressible flow started from an 'incompatible' initial condition has a sufficiently sound mathematical basis. This and the relation of this topic with PPE systems prompts research question III: *What is the near-wall behaviour of a solution of the Navier Stokes equations obtained in typical DNS, in particular the behaviour of the pressure gradient near the wall at $t = 0$ and in the chaotic turbulent regime?* To answer this question, we will revisit DNS of incompressible turbulent plane channel flow at $Re_\tau = 180$ [18, 19, 20, 21, 22, 23, 24, 25, 26]. We will precisely define the initial boundary value problem solved by the DNS, and show accurate and well-validated results that focus on the research questions above.

The same staggered projection method is used for the investigations of both research questions II and III. This projection method is embedded into a low-storage explicit second-order Runge-Kutta scheme. The pressure is frequently only first-order accurate in projection or fractional step methods [13, 14, 27, 28], but it will be shown that the second-order temporal accuracy of the present method is second-order, provided the pressure at time level n is not identified with the pressure computed in the last stage of time step n , but with the pressure computed in the first stage of the next time step (specifying the time level on the Poisson equation with right-hand side r , p^{n+1} is defined by $\nabla^2 p^{n+1} = r^{n+1} = r^{n+1,0}$; that Poisson equation is solved in the first stage of the next time step). This result was obtained independently of a recent and interesting paper of Sande & Koren [14], where the same notion can be found. The result is important in the present context, because it shows that it is possible to use the projection method to compute the pressure at time zero.

The main new points of the present paper are related to the above three research questions:

1. There exists a pressure Poisson equation system (PPE3), which is based on the standard Poisson equation (4) with Neumann pressure boundary condition (5). The additional near wall condition makes PPE3 equivalent to NS for smooth solutions, and a simple implementation of PPE3, which does not involve Green's functions, exists.
2. An analytical derivation and a numerical verification that a straightforward discretization of PPE3 on a staggered mesh is equivalent to the staggered discretization of NS (projection method) and to the staggered discretization of PPE2. The derivation of these equivalences shows how the staggered projection method, which does not need a pressure boundary condition, is related to PPE systems, which do need a (derived) pressure boundary condition. The derivation also sheds light on the PPE paradox and leads to an approximation of the wall value of $\partial p / \partial n$, which is not required but implied by the projection method.

3. A numerical investigation of the regularity properties described by H1980 by means of accurate and well-validated DNS of plane channel flow that develops from a clearly prescribed three-dimensional initial condition into a fully developed turbulent flow. The numerical solution appears to have the properties of the (possibly non-unique) solution described by H1980, in particular spatial continuity of the time derivative on the wall (H1980c): the vector equation $\nabla p = \nu \nabla^2 \mathbf{u} + \mathbf{f} - \mathbf{u} \cdot \nabla \mathbf{u} - \partial \mathbf{u} / \partial t$ on Γ , initially violated, appears to be valid immediately after $t = 0$, and also in the turbulent regime. In fact the numerical results indicate stronger regularity than described in H1980; the only discontinuities observed are those of the tangential viscous terms and the time derivatives of the tangential velocities on the wall at $t = 0$. The numerical results also indicate that HR1982 is correct and Lemma 3 in Ref. [8] is not correct, as in the limit $t \rightarrow 0$ the pressure gradient is shown to converge to the initial pressure gradient in the maximum norm, which is even stronger than HR1982.

The remainder of this paper is organized as follows. In section 2 we will present the discretization of system NS by an explicit projection method on a staggered grid. In section 3, we will analyze the equivalences between NS and the PPE systems, first for the continuous case and then more extensively for the discrete cases (research questions I and II). In sections 4-5, a specific channel flow case will be considered. In section 4, the simulation cases will be defined, and the spatial and temporal accuracy of the projection method of section 2 will be validated. In section 5, the discrete equivalence between PPE3 and NS will be numerically verified and the pressure boundary condition provided by PPE3 will be evaluated in a DNS (research question II). Furthermore, the near-wall behaviour of the pressure gradient and other terms of the Navier-Stokes equation will be numerically investigated both in the limit $t \rightarrow 0$ and in the turbulent regime, and theorems H1980 and HR1982 will be revisited using the DNS results (research question III). Conclusions will be presented in section 6.

2. An explicit projection method on a staggered grid

2.1. Temporal discretization

For the time integration in projection methods it is common to use the explicit second-order Adams-Bashforth method for the convective terms and the implicit second-order Crank-Nicolson method for the viscous terms, see e.g. [13, 29, 30]. Due to the time splitting error, the pressure is then not the true pressure but a pseudo-pressure. Several authors [13, 27, 28] demonstrated that the formal temporal accuracy of the Adams-Bashforth / Crank-Nicolson method is only first-order in wall-bounded flows. Perot [13] proposed an improvement that made the velocity second-order, but the pseudo-pressure remained first-order accurate in time. A second-order prediction of the pressure can be obtained after a correction with a term proportional to the Laplacian of the pseudo-pressure [31].

Two drawbacks of the Adams-Bashforth method are that it is not self-starting (\mathbf{u}^{n-1} is required) and unconditionally unstable in the inviscid limit. These limitations are overcome in a frequently employed variant, in which the convective terms are treated with an explicit Runge-Kutta method [32, 33, 34], and according to the latter two references, the pressure at the new time level is then identified with the pressure computed in the last stage of the time step. Several computations of incompressible flow have been performed with an explicit Runge-Kutta method applied to both convective and viscous terms [26, 14]. Runge-Kutta methods are self-starting, have no time-splitting errors if the pressure is computed in each stage, have in general good stability properties, and can be made higher-order accurate in time, also for the pressure [14].

The present projection method is embedded in a low-storage Runge-Kutta scheme with Runge-Kutta coefficients α_m ($m = 0, \dots, M - 1$), and associated coefficients $\alpha'_m = \alpha_m \Delta t$. Each time step $n + 1$ corresponds to $\Delta t = t^{n+1} - t^n$ and consists out of M stages. The time levels of the stages are denoted by $t^{n,m}$, where $t^{n,0} = t^n$ and $t^{n,m+1} = t^{n,0} + \alpha'_m$ for $0 \leq m < M$. Thus $t^{n,M} = t^{n+1}$, provided $\alpha_{M-1} = 1$. A quantity superscripted with n, m is evaluated at time $t^{n,m}$. At the beginning of each time step the start velocity field \mathbf{u}^n at time t^n is stored as $\mathbf{u}^{n,0}$. Then M stages follow. Stage number $m + 1$ ($0 \leq m < M$) contains three substeps:

1. compute the intermediate velocity

$$\mathbf{u}^* = \mathbf{u}^{n,0} + \alpha'_m [-\mathbf{u}^{n,m} \cdot \nabla \mathbf{u}^{n,m} + \nu \nabla^2 \mathbf{u}^{n,m} + \mathbf{f}^{n,m}]; \quad (10)$$

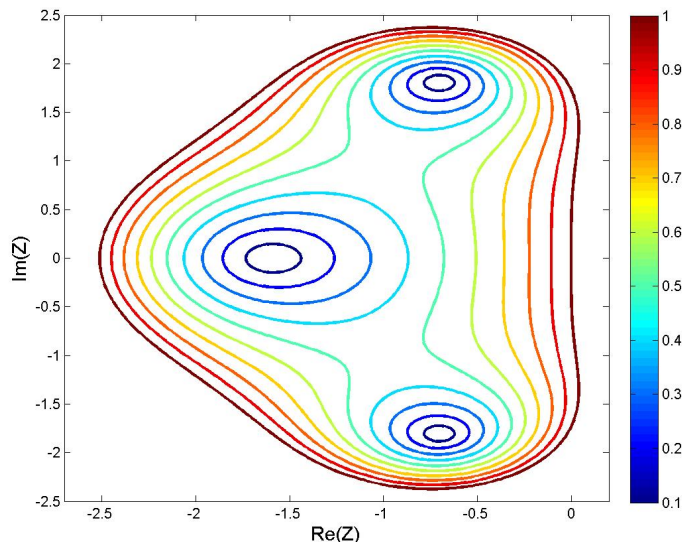


Figure 1: Stability regime for the low-storage three-stage RK method with coefficients $\alpha_0 = 1/3$, $\alpha_1 = 1/2$, and $\alpha_2 = 1$.

2. solve the Poisson equation

$$\nabla^2 p^{n,m} = (\nabla \cdot \mathbf{u}^*) / \alpha'_m; \quad (11)$$

3. update the velocity

$$\mathbf{u}^{n,m+1} = \mathbf{u}^* - \alpha'_m \nabla p^{n,m}. \quad (12)$$

The velocity \mathbf{u}^{n+1} at the new time level is equal to $\mathbf{u}^{n,M}$. The unconventional element in this scheme is that the pressure computed in stage m is labeled with index m instead of $m + 1$, although the latter is common in literature, see for example [33, 34]. In the present paper, the pressure at time t^n is defined by $p^n = p^{n,0}$. With this definition of p^n , not only the velocity, but also the pressure signal satisfies the formal order of accuracy of the Runge-Kutta method, provided the normal velocity on Γ is time-independent [14]. The definition implies that at the end of a time step the pressure at level $n + 1$ is not known yet; it becomes available in the first stage of the next time step.

For the simulations in this paper, a three-stage Runge-Kutta method ($M = 3$) was chosen, with $\alpha_0 = 1/3$, $\alpha_1 = 1/2$ and $\alpha_2 = 1$. This low-storage scheme is third-order accurate for linear and second-order accurate for nonlinear systems. The M -stage Runge-Kutta method for general coefficients α_m can be found in Ref. [35]. The Taylor expansion and the requirement of M^{th} -order accuracy for linear systems imply the coefficients $\alpha_m = 1/(M - m)$, where $M = 2$ recovers modified Euler, $M = 3$ the three-stage method, and $M = 4$ the four-stage method in Jameson & Baker [36]. The four-stage method, also second-order accurate, has successfully been applied in DNS of turbulent flows [37, 38]. The stability region of the three-stage method is defined by $|1 + \alpha_2 Z + \alpha_1 \alpha_2 Z^2 + \alpha_0 \alpha_1 \alpha_2 Z^3| \leq 1$ and shown in Fig. 1. Since the imaginary axis is inside the stability region for $\text{Im}(z) \leq 3^{1/2}$, $3^{1/2}$ is the maximum Courant number for stability in the inviscid limit. There are several third-order accurate three-stage Runge-Kutta schemes [14], but the simplicity of this particular three-stage scheme is appealing.

2.2. Spatial discretization

The spatial discretization is defined on a staggered grid, where the pressure and velocity divergence are defined at cell centers and the velocity components at cell faces [10]. Staggered finite difference methods have several advantages above collocated finite difference and spectral methods. Unlike collocated finite difference methods, staggered methods lead to a strong coupling of neighbouring pressure points without additional treatment. For the simulation of flows in complex geometries, finite difference methods are much more flexible than spectral methods. The staggered second-order scheme [10] has been generalized to higher order [39, 23], to body-fitted grids [40] and is also frequently used in immersed boundary

methods for flows with complex geometrical features [41]. In the present study the staggered second-order scheme is used [10]. The interpolation of the convective velocities is such that the convective scheme is also energy-conserving on a nonuniform grid [23].

We consider a staggered grid that is uniform in the x - and z -direction (mesh spacings h_x and h_z), but nonuniform in the wall-normal direction, the y -direction. Let N be the number of cells in the y -direction. The staggered grid locations where v is defined are given by

$$y_{s,j} = \frac{1}{2}L_y(1 + \tanh(-\gamma + 2\gamma j/N)/\tanh(\gamma)), \quad j = 0, \dots, N, \quad (13)$$

where the end locations ($j = 0, N$) coincide with a wall. The cell-center locations are defined by

$$y_{c,j} = \frac{1}{2}L_y(1 + \tanh(-\gamma + 2\gamma(j - \frac{1}{2})/N)/\tanh(\gamma)), \quad j = 0, \dots, N + 1, \quad (14)$$

where $j = 1, \dots, N$ refers to the cells inside the domain. The last equation also defines the cell-center locations of a layer of ghost-cells outside the domain ($y_{c,0}$ and $y_{c,N+1}$). The grid spacing in the normal direction is defined by

$$h_{c,j} = y_{s,j} - y_{s,j-1}, \quad j = 1, \dots, N, \quad (15)$$

$$h_{s,j} = y_{c,j+1} - y_{c,j}, \quad j = 0, \dots, N + 1. \quad (16)$$

The stretched grid is smooth in the entire domain also near the wall, and we will clarify that this property is crucial for the computation of the near-wall limit.

The discrete \mathbf{u} is defined on the entire grid, which means that the tangential velocities u and w are also defined at the ghost-cells at $j = 0$ and $j = N + 1$, and that the normal velocity v is also defined on the walls ($j = 0, N$). For an efficient implementation of the viscous terms in an explicit method, the concept of ghost-cells is very convenient, since it leads to an identical structure of the discretization at each internal point. However, it is stressed that the ghost-cells are not used for the pressure $p^{n,m}$, which is therefore only defined at internal points ($1 \leq j \leq N$).

The convective terms are discretized in the momentum-conserving divergence form (derived from the finite volume approach). For example, the term $\partial v^2/\partial y$ in the v -equation, required at y -location $y_{s,j}$, is discretized by

$$[\frac{1}{4}(v_j + v_{j+1})^2 - \frac{1}{4}(v_{j-1} + v_j)^2]/h_{s,j}. \quad (17)$$

It is remarked that the other convective derivatives with respect to y , $\partial(vu)/\partial y$ and $\partial(vw)/\partial y$, are independent of the wall values u_Γ and w_Γ in case the normal wall velocity v_Γ equals zero. The divergence form of the convective terms requires velocities to be interpolated from one staggered location to the cell-face of the same or another velocity component. All interpolations to obtain velocities on cell faces are simple averages over two adjacent points. The weights of these averages are $\frac{1}{2}$ and $\frac{1}{2}$ for the velocities in the seven derivatives $\partial(uu)/\partial x$, $\partial(vu)/\partial y$, $\partial(wu)/\partial z$, $\partial(uw)/\partial x$, $\partial(vw)/\partial y$, $\partial(wv)/\partial z$, and $\partial(vv)/\partial y$. In the discretization of $\partial(uw)/\partial x$, v is also interpolated with the weights $\frac{1}{2}$ and $\frac{1}{2}$, but the convective velocity u is interpolated by $(h_{c,j}u_j + h_{c,j+1}u_{j+1})/2h_{s,j}$, which can be deduced from the finite volume formulation in Ref. [23]. The latter interpolation rule is also used for the convective velocity w in $\partial(wv)/\partial z$. The selected interpolations lead to an energy-conserving convective scheme on the present nonuniform grid (this was verified, see section 4.2).

Turning to the viscous terms, the x - and z -derivatives in the velocity Laplacians are discretized with the compact second-order stencil (three points). For example, $\partial^2 u/\partial x^2$ is discretized as $B_{u,x} = (u_{i-1} - 2u_i + u_{i+1})/h_x^2$. With respect to the derivatives in the y -direction, $\partial^2 u/\partial y^2$ is discretized as

$$(B_{u,y}u)_j = [\frac{u_{j+1} - u_j}{h_{s,j}} - \frac{u_j - u_{j-1}}{h_{s,j-1}}]/h_{c,j}, \quad (18)$$

and similarly $B_{w,y}w$ approximates $\partial^2 w/\partial y^2$. Further, $\partial^2 v/\partial y^2$ is discretized as

$$(B_{v,y}v)_j = [\frac{v_{j+1} - v_j}{h_{c,j+1}} - \frac{v_j - v_{j-1}}{h_{c,j}}]/h_{s,j}. \quad (19)$$

The subscripts u , v or w in the operator B denote that the result of the discrete operator is defined on staggered u , v or w locations, respectively.

N	Extrapolation (20)	Extrapolation (21)
64	-2.00127	-1.5295
128	-2.00032	-1.5147
256	-2.00008	-1.5073

Table 1: Results for discretization (18) applied to $y(2-y)$ in cell $j=1$ for two different extrapolations at the wall. The analytical value equals -2 . Results are shown for three resolutions, in each case $\gamma=1.4$.

Since the wall at $y_{s,N}$ is treated in the same way as the wall at $y_{s,0}$, it suffices to limit the presentation of the velocity boundary condition to the wall at $y_{s,0}$. The wall boundary condition for v is straightforward: $v_0 = v_\Gamma$. Since, unlike the discrete v , the discrete u and w are not defined on the walls, the discretization of the boundary conditions for u and w on the wall at $y_{s,0}$ is more complicated and involves the ghost-cells at $y_{c,0}$. The velocities u and w in these ghost-cells are determined by a fourth-order extrapolation,

$$u_0 = u_\Gamma + \beta_1(u_1 - u_\Gamma) + \beta_2(u_2 - u_\Gamma) + \beta_3(u_3 - u_\Gamma). \quad (20)$$

The grid-dependent coefficients β_1 , β_2 and β_3 are specified in Appendix 1. With Eq. (20) the approximation of $\partial^2 u / \partial y^2$ is locally second-order in the entire domain, provided the stretching function is smooth and its derivative is nonzero (also across the wall).

The standard second-order (linear) interpolation,

$$u_0 = 2u_\Gamma - u_1 \quad \text{and} \quad y_{c,0} = -y_{c,1}, \quad (21)$$

is not used, because it leads to zeroth-order local accuracy of $\partial^2 u / \partial y^2$ near the wall [3, 5]. This is unsuitable for our purpose to study the near-wall limit. As an example, Table 1 shows results for $\partial^2 u / \partial y^2$ with $u = y(2-y)$ in the point $y_{c,1}$ approximated by (18) using extrapolations (20) and (21) on three different grids. Both cases seem to converge with grid-refinement, but only extrapolation (20) converges to the correct value near the wall. It is remarked that the global truncation error (the error in \mathbf{u} and p) is second-order accurate, also if the standard extrapolation (21) is used [42].

With the definition of the convective and viscous schemes the intermediate velocity \mathbf{u}^* can be obtained at all internal grid points. We proceed with the discretization of the Poisson equation. The discrete pressure gradient operator is denoted by $\mathbf{G} = (G_x, G_y, G_z)$, while the discrete divergence operator is denoted by $\mathbf{D} = (D_x, D_y, D_z)$. The discretized form of the Poisson equation reads

$$\mathbf{D} \cdot \mathbf{G} p^{n,m} = (\mathbf{D} \cdot \mathbf{u}^*) / \alpha'_m. \quad (22)$$

The operators D_x , D_z , G_x , G_z do not interfere with the walls. In the normal direction, the operators are defined by

$$(G_y p^{n,m})_j = (p_{j+1}^{n,m} - p_j^{n,m}) / h_{s,j}, \quad j = 1, \dots, N-1, \quad (23)$$

and

$$(D_y v^*)_j = (v_j^* - v_{j-1}^*) / h_{c,j}, \quad j = 1, \dots, N. \quad (24)$$

The discretization of $\partial^2 p / \partial y^2$ in the Poisson equation equals $D_y G_y p^{n,m}$. It can be convenient to use a modified definition of D_y near the walls [6, 13, 14], but we prefer not to do so, to keep the structure of the discrete Poisson equation as close as possible to the structure of a continuous Poisson equation. As a consequence, Poisson equation (22) involves $(G_y p^{n,m})_\Gamma$ and v_Γ^* , the values of v^* and $G_y p^{n,m}$ at $j=0$ and $j=N$, which have not yet been defined.

Before we specify the latter two quantities, we discretize the third substep of the projection method,

$$\mathbf{u}^{n,m+1} = \mathbf{u}^* - \alpha'_m \mathbf{G} p^{n,m}, \quad (25)$$

which is used to obtain the new velocity $\mathbf{u}^{n,m+1}$ at all internal grid points. It is not used to obtain the normal velocity $v^{n,m+1}$ on the walls, since these values are directly provided by the prescribed velocity boundary condition v_Γ at $t^{n,m+1}$. In the execution of the third substep, the pressure gradient $\mathbf{G} p^{n,m}$ needs to be computed at internal points only.

The momentum balance in the projection method is expressed by the third substep. A continuous solution of the velocity acceleration requires the momentum balance to be satisfied on the walls as well. Since (25) is not required to update the velocity at the wall, it is used to define the relation between the wall values of $G_y p$ and v^* , which implies [3]

$$(G_y p^{n,m})_\Gamma = (v_\Gamma^* - v_\Gamma^{n,m+1})/\alpha'_m. \quad (26)$$

This is the Neumann boundary condition used for the Poisson equation in the projection method formulated with unmodified definition of \mathbf{D} . With definition (26), the discrete momentum balance (25) for v also holds on Γ . Since (25) is now satisfied for $0 \leq j \leq N$, we can apply the discrete divergence operator to (25), which yields

$$\mathbf{D} \cdot \mathbf{u}^{n,m+1} = \mathbf{D} \cdot \mathbf{u}^* - \alpha'_m \mathbf{D} \cdot \mathbf{G}p = 0, \quad (27)$$

in all internal cells, provided Poisson equation (22) is satisfied in all internal cells.

An essential feature of the explicit projection method is that the numerical solution is independent of the value of v_Γ^* , see section 6.3.1 in [3]. This is also the case for the present multistage method; if we write out Poisson equation (22) at $y_{c,1}$, move $-(G_y p^{n,m})_\Gamma/h_{c,1}$ to the right-hand side and substitute (26), the term with v_Γ^* cancels and we obtain

$$D_x G_x p^{n,m} + \frac{(p_2^{n,m} - p_1^{n,m})}{h_{s,1} h_{c,1}} + D_z G_z p^{n,m} = (D_x u^* + \frac{v_1^* - v_\Gamma^{n,m+1}}{h_{c,1}} + D_z w^*)/\alpha'_m, \quad (28)$$

which shows that the solution $p^{n,m}$ in the interior of the domain does not depend on $v_\Gamma^* = v_0^*$. Equation (28) clearly shows that the staggered discretization does not need a pressure boundary condition.

Equation (28) can also be directly derived from the staggered discretization of the primitive equations [3, 6, 13, 14]. It is remarked that (28) has not the form of a Poisson equation, since the left-hand side does not represent the true value of $\nabla^2 p^{n,m}$ at $y_{c,1}$. Strictly speaking, (28) is not a discrete Poisson equation, we need to take one step to transform (28) into a discrete formal Poisson equation. This has not a practical purpose, since (28) is quite convenient to define the coefficient matrix and the right-hand side of the implicit pressure equation solved in practice. To take this formal step is nonetheless useful, since it will give us information about the underlying continuous PPE problem. So starting from (28), how is this last formal step taken? Subtract $-(G_y p^{n,m})_\Gamma/h_{c,1}$ from both sides of (28), and substitute for $(G_y p^{n,m})_\Gamma$ on the right-hand side a discrete Neumann boundary condition. How is this boundary condition obtained? In case of the projection method, it is simply derived from the requirement that the normal momentum equation (25) should be satisfied on the walls, which leads to (26). Thus the reasoning in the discrete case is entirely analogous to the reasoning in the continuous case. The continuous Navier-Stokes equations do not need a pressure boundary condition, but the derivation of a Poisson equation from the Navier-Stokes equations increases the order of the system and therefore additional boundary conditions are needed, boundary conditions that should be derived from the original Navier-Stokes problem, or more precisely from suitable regularity conditions imposed on the Navier-Stokes equations. For example, the Neumann pressure boundary condition follows from requirement that $\partial v/\partial t$ should be continuous in space on $\bar{\Omega}$ (which includes Γ).

Since the numerical solution is independent of v_Γ^* , any value can be chosen for v_Γ^* . For the simulations in the present paper $v_\Gamma^* = v_\Gamma^{n,m+1}$ was used. This choice is convenient, since the Poisson equation can then be solved with the simple homogeneous Neumann condition, $(G_y p^{n,m})_\Gamma = 0$. For $v_\Gamma^* = v_\Gamma^{n,m+1}$, Eq. (22) is not only equivalent to Eq. (28), but directly reduces to it. Although the solution in the interior does not depend on v_Γ^* , $(G_y p^{n,m})_\Gamma$ does depend on v_Γ^* . Therefore, for most choices of v_Γ^* , including $v_\Gamma^* = v_\Gamma^{n,m+1}$, the corresponding $(G_y p^{n,m})_\Gamma$ defined by (26) does not represent the physical pressure gradient on the wall. Which definition of v_Γ^* does provide a physical value of $(G_y p^{n,m})_\Gamma$ will become clear in the next section.

The solution (\mathbf{u}^n, p^n) at t^n is equal to $(\mathbf{u}^{n,0}, p^{n,0})$, which is available when the Poisson equation in the first stage of a time-step has been solved. If the field at t^n is needed for post-processing, this is the moment to write it to file. Alternatively one could compute p^n at t^n by solving an additional Poisson equation at the end of time step n and then skip the computation of $p^{n,0}$, which was actually preferred in Ref. [14]. The present variant has the advantage that memory can be saved, since there is no need to store the pressure during the computation of the convective and viscous terms.

In this work, the discrete Poisson equation was solved down to machine precision by a direct method, FFT for the homogeneous directions and the inversion of the tri-diagonal matrix in the normal direction by two sweeps of Gauss-elimination. As a result, the divergence of the velocity $\mathbf{u}^{n,m}$ was zero down to machine precision (after the wall-boundary condition to $v^{n,m}$ in substep 1 was applied). The spatial integral of the solution of the Poisson equation was set to zero by subtracting the spatial average. The discrete integral of the pressure was defined as a summation over all grid cells after multiplication of the cell-centered value with the local cell-volume $h_x h_{c,j} h_z$.

3. Equivalence between NS and PPE systems

To investigate the issues addressed in research questions I and II formulated in the Introduction, we analyze the smooth and discrete equivalence between NS and several PPE systems, with a focus on PPE systems with the Neumann pressure boundary condition.

3.1. Smooth equivalence

Although, as explained in the Introduction, solutions of system NS and the PPE systems are not necessarily smooth, it is instructive to analyze 'smooth equivalence', *i.e.* the equivalence of the systems for smooth solutions. The four PPE systems, PPE0-3 defined in the Introduction, have all been derived from NS by differentiation and combination of the equations and boundary conditions. Therefore, a smooth solution of NS is also a solution of the four PPE systems.

Reversely, suppose that (\mathbf{u}, p) is a smooth solution of one of the four PPE systems. The systems PPE0, PPE1 and PPE3 have the same Poisson equation (4), but different boundary conditions. For a smooth solution (\mathbf{u}, p) of one of these systems, subtracting (4) from the divergence of the momentum equation leads to

$$\frac{\partial}{\partial t} \nabla \cdot \mathbf{u} = \nu \nabla^2 (\nabla \cdot \mathbf{u}) \quad (29)$$

defined in Ω [7]. For PPE0, this divergence diffusion equation implies $\nabla \cdot \mathbf{u} = 0$ for all t , since PPE0 imposes $\nabla \cdot \mathbf{u} = 0$ on Γ and $\nabla \cdot \mathbf{u}^0 = 0$ [7]. Therefore, a smooth solution (\mathbf{u}, p) of PPE0 is also a smooth solution of NS. For PPE1, the divergence diffusion equation does not imply that $\nabla \cdot \mathbf{u} = 0$ remains zero for all times; nonzero divergence might emerge on the wall and then diffuse into the interior of the domain. An example of a smooth solution that does not remain divergence free can be found in section 3.10.3 in Ref. [7], for a PPE1 problem based on the Stokes equations. System PPE2 uses another Poisson equation, Eq. (6). Application of the divergence to the momentum equation (2) and subtracting (6) leads to $\partial(\nabla \cdot \mathbf{u})/\partial t = 0$ for all t . Since $\nabla \cdot \mathbf{u} = 0$ at $t = 0$ and the solution is assumed to be smooth, $\nabla \cdot \mathbf{u} = 0$ for all t is implied; a smooth solution (\mathbf{u}, p) of PPE2 is also a solution of NS [7].

For PPE3, constraint Eq. (7) implies $\nabla^2 \nabla \cdot \mathbf{u} = 0$ in the neighbourhood of Γ . It follows from Eq. (29) that $\partial(\nabla \cdot \mathbf{u})/\partial t = 0$ in that neighbourhood, and hence $\nabla \cdot \mathbf{u} = 0$ for all t in the same neighbourhood, since also $\nabla \cdot \mathbf{u}^0 = 0$. Equation (29) with zero value of $\nabla \cdot \mathbf{u}$ in a neighbourhood of Γ and $\nabla \cdot \mathbf{u}^0 = 0$ implies $\nabla \cdot \mathbf{u} = 0$ in Ω for all t . So a smooth solution (\mathbf{u}, p) of PPE3 is also a solution of NS. We conclude that PPE3 is smoothly equivalent to NS, like PPE0 and PPE2.

If two systems A and B are equivalent and A has a unique solution (is well-posed), B has also a unique solution; the equivalence implies that B has at least one solution and if B had multiple solutions, A would also have multiple solutions, such that the solution of A would not be unique.

Important differences between PPE3 and the other PPE systems can be expressed as follows. Whereas PPE0 requires Green's functions to obtain the (Dirichlet) boundary condition of the Poisson equation, PPE3 uses the Neumann boundary condition, which is much simpler to evaluate. Whereas PPE1 is not smoothly equivalent to NS, PPE3 is. Whereas PPE2 needs the paradoxical inclusion of the viscous term in the Poisson equation (PPE paradox), PPE3 does not require this paradoxical term.

As indicated in the Introduction, the formulation of system NS is such that the solution is not necessarily smooth. Formal equivalence between PPE3 (or PPE0 or PPE2) and NS for non-smooth solutions seems to be a much more complicated problem than the equivalence for smooth solutions. Instead of that question, we will address a related but simpler question: Is it possible to prove discrete equivalence, *i.e.* equivalence between suitable discretizations of PPE systems and the discretization of system NS (the projection method of section 2)?

3.2. Discrete equivalence

The discrete equivalence between NS and PPE systems will be presented in the following order. After discussing the constraint on the initial divergence, we will consider a discretization of the primitive equations (the MAC method), the projection method, a discretization of PPE2, and finally a discrete version of PPE3. The equivalence of these four discrete systems will be discussed and proven, if required.

The derivation of a PPE involves a spatial differentiation of the momentum equation, but also a temporal differentiation of the continuity equation. Due to the latter, a PPE system needs an additional initial condition, which is $\nabla \cdot \mathbf{u} = 0$ at $t = 0$ (see the literature on discrete algebraic equations, for example [7]). Although the physical condition $\nabla \cdot \mathbf{u}^0 = 0$ is also assumed for system NS, this is formally not necessary; without this property, the (discontinuous) solution of NS will still satisfy $\nabla \cdot \mathbf{u} = 0$ for $t > 0$, since that equation is imposed for $t > 0$. We recognize this feature of NS in the projection method: after one stage the discrete divergence is zero, even if the initial velocity field is not divergence free. For a PPE system, however, a divergence free velocity for $t > 0$ can only be obtained if the integration is started from a divergence-free velocity at $t = 0$ [7]. If we had defined NS without $\nabla \cdot \mathbf{u}^0 = 0$, then the initial condition $\nabla \cdot \mathbf{u}^0 = 0$ in the PPE system would follow from the regularity requirement that $\nabla \cdot \mathbf{u}$ should be continuous on $[0, \infty) \times \Omega$. Thus for the discrete PPE systems we require that the discrete divergence of the initial velocity is zero, $\mathbf{D} \cdot \mathbf{u}^{0,0} = 0$. Unlike the discretization of NS by the projection method, a discretization of a PPE system needs this to produce a solution with zero discrete divergence down to machine precision.

The MAC method is a direct discretization of system NS on a staggered grid. It does not involve a definition of a pressure boundary condition on Γ . Stage $m + 1$ ($0 \leq m < M$) of the present Runge-Kutta method applied to the MAC method can be described as follows. First the ghost-cell values of $u^{n,m}$, $w^{n,m}$ and the wall values of $v^{n,m}$ are set. Also the wall values of $v^{n,m+1}$ are set. The discrete continuity and momentum equations at *internal* points are:

$$\mathbf{D} \cdot \mathbf{u}^{n,m+1} = 0, \quad (30)$$

$$\mathbf{u}^{n,m+1} - \mathbf{G}p^{n,m} = \mathbf{u}^{n,0} + \alpha'_m[-\mathbf{a}^{n,m} + \mathbf{b}^{n,m} + \mathbf{f}^{n,m}]. \quad (31)$$

The symbols $\mathbf{a}^{n,m}$ and $\mathbf{b}^{n,m}$ refer to the discretizations of the convective and viscous terms, respectively, and also include the implementation of the no-slip boundary condition as described in section 2.2. The vector of unknowns consists out of the *internal* values of $(\mathbf{u}^{n,m+1}, p^{n,m})$. Most known terms appear on the right-hand side, but the known terms in the continuity equation (the boundary value of the normal velocity $v_\Gamma^{n,m+1}$) are kept on the left-hand side, since we prefer the use of an unmodified \mathbf{D} , as explained in section 2.2. Since the continuity equation is defined at the same locations as the pressure, the number of unknowns in (30-31) is the same as the number of equations; in principle (30-31) can be solved directly.

The structure of stage $m + 1$ of the projection method is (section 2.2):

$$\mathbf{u}^* = \mathbf{u}^{n,0} + \alpha'_m[-\mathbf{a}^{n,m} + \mathbf{b}^{n,m} + \mathbf{f}^{n,m}], \quad (32)$$

$$(G_y p^{n,m})_\Gamma = (v_\Gamma^* - v_\Gamma^{n,m+1})/\alpha'_m, \quad (33)$$

$$\mathbf{D} \cdot \mathbf{G}p^{n,m} = (\mathbf{D} \cdot \mathbf{u}^*)/\alpha'_m, \quad (34)$$

$$\mathbf{u}^{n,m+1} = \mathbf{u}^* - \alpha'_m \mathbf{G}p^{n,m}. \quad (35)$$

All known quantities are on the right-hand sides, except v_Γ^* , but $\mathbf{u}^{n,m+1}$ and $p^{n,m}$ do not depend on this quantity. The projection method is equivalent to the MAC method, since it can be derived from the MAC method and vice-versa [3, 6, 13, 14].

Next we proceed with the PPE systems. For these systems we need to assume $\mathbf{D} \cdot \mathbf{u}^{0,0} = 0$, which is not required for the MAC and the projection method. The discrete PPE2 on a staggered grid is given by

$$\mathbf{d}^* = -\mathbf{a}^{n,m} + \mathbf{b}^{n,m} + \mathbf{f}^{n,m}, \quad (36)$$

$$(G_y p^{n,m})_\Gamma = d_\Gamma^* - (v_\Gamma^{n,m+1} - v_\Gamma^{n,0})/\alpha'_m, \quad (37)$$

$$\mathbf{D} \cdot \mathbf{G}p^{n,m} = (\mathbf{D} \cdot \mathbf{d}^*)/\alpha'_m, \quad (38)$$

$$\mathbf{u}^{n,m+1} = \mathbf{u}^{n,0} + \alpha'_m(\mathbf{d}^* - \mathbf{G}p^{n,m}). \quad (39)$$

If $\mathbf{D} \cdot \mathbf{u}^{n,0} = 0$, the application of the discrete divergence operator to the last equation yields $\mathbf{D} \cdot \mathbf{u}^{n,m+1} = 0$ at points where the discrete divergence is defined. Since $\mathbf{D} \cdot \mathbf{u}^{0,0} = 0$ by definition, an induction argument implies $\mathbf{D} \cdot \mathbf{u}^{n,m} = 0$ for all n, m . Like the projection method does not depend on v_Γ^* , the discrete PPE2 does not depend on $(d_y^*)_\Gamma$, the boundary value of the normal component of \mathbf{d}^* .

System PPE3 discretized on a staggered grid is given by

$$\mathbf{a}^* = -\mathbf{a}^{n,m} + \mathbf{f}^{n,m}, \quad (40)$$

$$(b_y^{n,m})_\Gamma = (b_y^{n,m})_1 + h_{c,1}(D_x b_x + D_z b_z)_1, \quad (41)$$

$$(G_y p^{n,m})_\Gamma = (b_y^{n,m})_\Gamma + a_\Gamma^* - (v_\Gamma^{n,m+1} - v_\Gamma^{n,0})/\alpha'_m, \quad (42)$$

$$\mathbf{D} \cdot \mathbf{G} p^{n,m} = (\mathbf{D} \cdot \mathbf{a}^*)/\alpha'_m, \quad (43)$$

$$\mathbf{u}^{n,m+1} = \mathbf{u}^{n,0} + \alpha'_m(\mathbf{a}^* - \mathbf{G} p^{n,m} + \mathbf{b}^{n,m}). \quad (44)$$

The second equation prescribes the boundary value of the normal component of the viscous term, which, in PPE3, is a direct consequence of the discretization of the zero divergence of the velocity Laplacian near the wall at location $y_{c,1}$. A similar equation imposed at $y_{c,N}$ provides the boundary value at $y_{s,N}$. Like the projection method and PPE2 do not depend on v_Γ^* and $(d_y^*)_\Gamma$, PPE3 does not depend on the boundary value $(a_y^*)_\Gamma$. Note that if the velocity on the boundary does not depend on time, the physical value for $(a_y^*)_\Gamma$ simply equals $(f_y)_\Gamma$, since the convective term on the boundary is then zero (see the remark below (5)).

Application of the discrete divergence to momentum equation (44) and subsequent substitution of the Poisson equation (43) implies the discrete divergence diffusion equation

$$\mathbf{D} \cdot \mathbf{u}^{n,m+1} = \mathbf{D} \cdot \mathbf{u}^{n,0} + \alpha'_m \mathbf{D} \cdot \mathbf{b}^{n,m}, \quad (45)$$

for Runge-Kutta stage $m + 1$. An important statement of the staggered viscous approximation of the viscous terms is:

$$\text{If } \mathbf{D} \cdot \mathbf{u}^{n,m} = 0 \text{ for } 1 \leq j \leq N, \text{ then } \mathbf{D} \cdot \mathbf{b}^{n,m} = 0 \text{ for } 2 \leq j \leq N - 1. \quad (46)$$

See Appendix 2 for a proof of this statement. If $\mathbf{D} \cdot \mathbf{u}^{n,m} = \mathbf{D} \cdot \mathbf{u}^{n,0} = 0$ in all cells, then this statement and (41) imply that $\mathbf{D} \cdot \mathbf{b}^{n,m} = 0$ in all cells, such that the discrete divergence diffusion equation (45) implies $\mathbf{D} \cdot \mathbf{u}^{n,m+1} = 0$. Since $\mathbf{D} \cdot \mathbf{u}^{0,0} = 0$ by definition, we have $\mathbf{D} \cdot \mathbf{u}^{n,m} = 0$ for all n, m .

The equivalences between the MAC method, the projection method, the discrete PPE2 and the discrete PPE3 can be proven by showing that the solution spaces are the same. We sketch such a proof for the equivalence between the projection method and PPE3. Suppose $(\mathbf{u}^{n,m}, p^{n,m})$ is a solution of the projection method. Then $\mathbf{D} \cdot \mathbf{u}^{n,m} = 0$. Define (40-42) and derive (43-44) from (32-35), (40-42) and from the fact that $\mathbf{D} \cdot \mathbf{b}^{n,m} = 0$, due to (41) and (46). Thus $(\mathbf{u}^{n,m}, p^{n,m})$ is also a solution of PPE3. Reversely, suppose $(\mathbf{u}^{n,m}, p^{n,m})$ is a solution of PPE3. Then $\mathbf{D} \cdot \mathbf{u}^{n,m} = 0$ and $\mathbf{D} \cdot \mathbf{b}^{n,m} = 0$ (proven above). Define (32-33) and derive (34-35) from (40-44). Thus the solution of PPE3 is also a solution of the projection method.

Comparing the projection method, PPE2, and PPE3, we see a remarkable structure. In fact each of these methods uses projection, but the scope of the projection is different in each case. In the projection method, the convective term plus forcing term plus viscous term plus old velocity divided by α'_m is projected to obtain a divergence free velocity. In PPE2, only the convective plus forcing plus viscous term is projected. In PPE3, only the convective plus forcing term is projected. In each case the discrete Neumann pressure boundary condition is derived from the discrete normal momentum equation on the boundary; the requirement that for the v -component (35), (39) or (44) should hold on Γ implies (33), (37) or (42), respectively. With each limitation of the scope of the projection, a new condition needs to be added. PPE2 and PPE3 skip the initial velocity from the projection scope, and therefore they need zero initial divergence of the velocity in order to obtain zero divergence for $t > 0$. PPE3 skips the viscous term from the projection scope, and therefore it needs zero divergence of the velocity Laplacian near the boundary to keep the velocity divergence free.

In each of these three cases only $(G_y p^{n,m})_\Gamma$ is influenced by the wall value of the projected term, v_Γ^* , d_Γ^* and a_Γ^* , respectively. The discrete internal solution $(\mathbf{u}^{n,m}, p^{n,m})$ does not depend on the wall value of the projected term; by substitution of $(G_y p^{n,m})_\Gamma$ into the Poisson equation not only $(G_y p^{n,m})_\Gamma$, but also

the wall value of the projected term can be eliminated. The equation after the eliminations is of course correct and very convenient in practice, but this equation has not the form of a direct discretization of a Poisson equation, since the left-hand side does not represent the physical $\nabla^2 p$ (see also the discussion after Eq. (28)).

3.3. Discussion

Next we discuss in some more detail implications of the previous section for the PPE paradox (why does PPE2 work while PPE1 does not?) and the physical pressure Neumann condition not required but implied by the projection method. In addition the pressure correction method (SMAC) will be discussed.

A discretization of PPE1 is obtained if (41) is replaced by

$$(b_y^{n,m})_\Gamma = b_\Gamma^* = \sum_{j=1}^J \zeta_j (b_y)_j, \quad (47)$$

which is a straightforward extrapolation of the discretized $\nu \nabla^2 v$ from the interior. Here J is an integer value, and ζ_j are coefficients such that a fourth-order approximation for $\nu \nabla^2 v$ on the wall is obtained. After the first stage in the first time step, $\mathbf{D} \cdot \mathbf{u}^{0,1}$ is zero for $2 \leq j \leq N-1$, which follows from $\mathbf{D} \cdot \mathbf{u}^{0,0} = 0$, statement (46) and equation (45). However, $\mathbf{D} \cdot \mathbf{u}^{0,1}$ will in general be nonzero at $y_{c,1}$, since statement (46) is in general not valid at $j=1$. In the next stage the velocity divergence will then become nonzero at $y_{c,2}$ and so forth. Thus nonzero divergence emerges in the internal cells adjacent to the wall and subsequently diffuses into the interior of the domain. This is the reason why the discrete PPE1 is not equivalent to the discrete NS, unlike PPE3.

Thus the constraint of zero divergence of the velocity Laplacian in PPE3 is an essential one, it can not simply be left out if the standard (simplified) Poisson equation (4) is used. The difference between PPE1 and PPE3 (see also section 5.4) shows that the appearance of the wall value of the viscous term b_y in the Neumann pressure boundary condition influences the internal solution. In this respect both PPE1 and PPE3 differ from PPE2 and the projection method, in which the numerical value of the viscous term in the definition of $(G_y p)_\Gamma$ does not matter. Compared to PPE1 and PPE3, due to the inclusion of the viscous term in the Poisson equation, PPE2 is more similar to the standard projection method and does not require an additional constraint on the divergence of the velocity or velocity Laplacian on or near the wall. In PPE2 (and in the projection method), it does not matter that, for arbitrary $(b_y)_\Gamma$, $\mathbf{D} \cdot \mathbf{b}$ is in general nonzero in the cells $j=1$ and $j=N$. In these cases, divergence errors induced by $\mathbf{D} \cdot \mathbf{b} \neq 0$ are automatically corrected in the projection step (when the pressure gradient is subtracted).

As indicated in the Introduction PPE2 has been criticized in literature, in the sense that the problems of PPE1 were also attributed to PPE2 [8]. Whereas this statement was already claimed to be unjustified in Ref. [9] by arguments that involved weak formulations of the Stokes equations, the presently shown discrete equivalence between PPE2 and NS can be viewed as a further justification of PPE2.

Another consequence of the equivalence between the discrete PPE3 and the projection method is that it reveals the discrete physical Neumann pressure boundary condition, which is not required by the projection method, but can be derived from the projection method. For time-independent velocity on Γ , the physical approximation of $(a_y^*)_\Gamma$ is simply $(f_y)_\Gamma$, and in the more general case, a physical approximation of this quantity is given by $-(a_y)_\Gamma + (f_y)_\Gamma$, where $(a_y)_\Gamma$ can be any consistent discretization of $\mathbf{u} \cdot \nabla v$ on Γ . Then the approximation of $(G_y p)_\Gamma$ in PPE3 is the physical approximation of the boundary value of $\partial p / \partial y$ implied by the standard projection method:

$$(G_y p^{n,m})_\Gamma = (b_y^{n,m})_\Gamma + (f_y^{n,m})_\Gamma - (a_y^{n,m})_\Gamma - (v_\Gamma^{n,m+1} - v_\Gamma^{n,0}) / \alpha'_m, \quad (48)$$

with $(b_y^{n,m})_\Gamma$ defined by (41). Since the projection method is equivalent to the discrete PPE3, the choice

$$v_\Gamma^* = v_\Gamma^{n,0} + \alpha'_m \left((b_y^{n,m})_\Gamma + (f_y^{n,m})_\Gamma - (a_y^{n,m})_\Gamma \right) \quad (49)$$

in the projection method and subsequent evaluation of (33) produces the same result as (48).

We finish this subsection with a discussion of the concept of pressure correction, proposed in the SMAC (simplified marker and cell) method [43]. It appears that the introduction of pressure correction

Simulation	System	$p(t^{n+1})$	Δt	Spatial resolution
A1	NS	$p^{n+1,0}$	0.002	$256 \times 128 \times 128$
A2	NS	$p^{n+1,0}$	0.001	$256 \times 128 \times 128$
A3	NS	$p^{n+1,0}$	0.0005	$256 \times 128 \times 128$
A3R	NS	$p^{n+1,0}$	0.0005	$512 \times 256 \times 256$
A4	NS	$p^{n+1,0}$	0.00025	$256 \times 128 \times 128$
B1	NS	$p^{n,2}$	0.002	$256 \times 128 \times 128$
B2	NS	$p^{n,2}$	0.001	$256 \times 128 \times 128$
B3	NS	$p^{n,2}$	0.0005	$256 \times 128 \times 128$
B4	NS	$p^{n,2}$	0.00025	$256 \times 128 \times 128$
C1	PPE1	$p^{n+1,0}$	0.002	$256 \times 128 \times 128$
D1	PPE3	$p^{n+1,0}$	0.002	$256 \times 128 \times 128$

Table 2: Overview of performed simulations.

does not make the analysis essentially different. Pressure correction can be embedded in the present projection method by reuse of the pressure $p^{n,m-1}$ computed in the previous stage after the definition of $t^{n,-1} = t^{n-1,M-1}$ and $p^{0,-1} = 0$. Then $\alpha'_m \mathbf{G} p^{n,m-1}$ is subtracted from \mathbf{u}^* in substep 1, $p^{n,m}$ is replaced by p' in substeps 2 and 3, and substep 3 is followed by the computation of $p^{n,m} = p^{n,m-1} + p'$. Clearly, p' is an approximation of $(t^{n,m} - t^{n,m-1})\partial p/\partial t$, except at $t = 0$. In pressure correction methods it is common to specify $\partial p'/\partial n = 0$ on a wall, see for example Ref. [44], although this is not proportional to the true value of $\partial^2 p/\partial n \partial t$ on Γ , because the true (physical) value is in general not zero. However, this is not a problem, provided the correct relation between the wall values of $G_y p'$ and v^* is specified (Eq. (26) with $p^{n,m}$ replaced by p'). Then the internal pressure does not depend on the wall values of $G_y p'$ and v^* , since these can be eliminated from the equations, like in the original projection method the wall values of $G_y p$ and v^* can be eliminated.

4. Numerical case definition and accuracy check

4.1. Case definition

In this section we define the turbulent plane channel flow simulated by DNS. The dimensions of the domain are the same as in Ref. [21], $L_x = 4\pi$, $L_y = 2$ and $L_z = 4\pi/3$. The no-slip condition is $\mathbf{u} = \mathbf{0}$ on Γ ($y = 0$ and $y = L_y$). The forcing term is given by $\mathbf{f} = (1, 0, 0)$. As a consequence $\bar{u}_\tau = 1$, where \bar{u}_τ is defined as $(\nu d\bar{u}/dy)^{1/2}$ evaluated on Γ , where $\bar{u}(y)$ is the mean streamwise velocity. The viscosity equals $\nu = 1/180$ and the Reynolds number equals $Re_\tau = \bar{u}_\tau L_y / 2\nu = 180$. The Reynolds number based on mean centerline velocity and L_y is approximately 6500. The viscous length-scale is defined by $\delta_\nu = \nu/\bar{u}_\tau = 1/180$. The normal coordinate in wall units is defined by $y_+ = y/\delta_\nu = 180y$.

The initial condition \mathbf{u}^0 is defined as

$$u^0 = ay(L_y - y) + b \sum_{k=1}^2 \cos \frac{2k\pi x}{L_x} \sin \frac{2k\pi y}{L_y} \sin \frac{2k\pi z}{L_z}, \quad (50)$$

$$v^0 = -\frac{bL_y}{2L_x} \sum_{k=1}^2 \sin \frac{2k\pi x}{L_x} (-1 + \cos \frac{2k\pi y}{L_y}) \sin \frac{2k\pi z}{L_z}, \quad (51)$$

$$w^0 = -\frac{bL_z}{2L_x} \sum_{k=1}^2 \sin \frac{2k\pi x}{L_x} \sin \frac{2k\pi y}{L_y} \cos \frac{2k\pi z}{L_z}, \quad (52)$$

with $a = 22.5$ and $b = a/10$. This velocity field is divergence free and satisfies the no-slip condition on the two walls. The discrete divergence of the initial velocity \mathbf{u}^0 defined above is only approximately zero (with a second-order spatial truncation error). Therefore the discrete initial velocity is defined by $\tilde{\mathbf{u}}^0 = \mathbf{u}^0 - \mathbf{G}\phi$, where ϕ is the solution of $\mathbf{D} \cdot \mathbf{G}\phi = \mathbf{D} \cdot \mathbf{u}^0$, such that $\mathbf{D} \cdot \tilde{\mathbf{u}}^0 = 0$. It is stressed that the variable ϕ is not the initial pressure but a purely numerical quantity. The correction $-\mathbf{G}\phi$ converges to

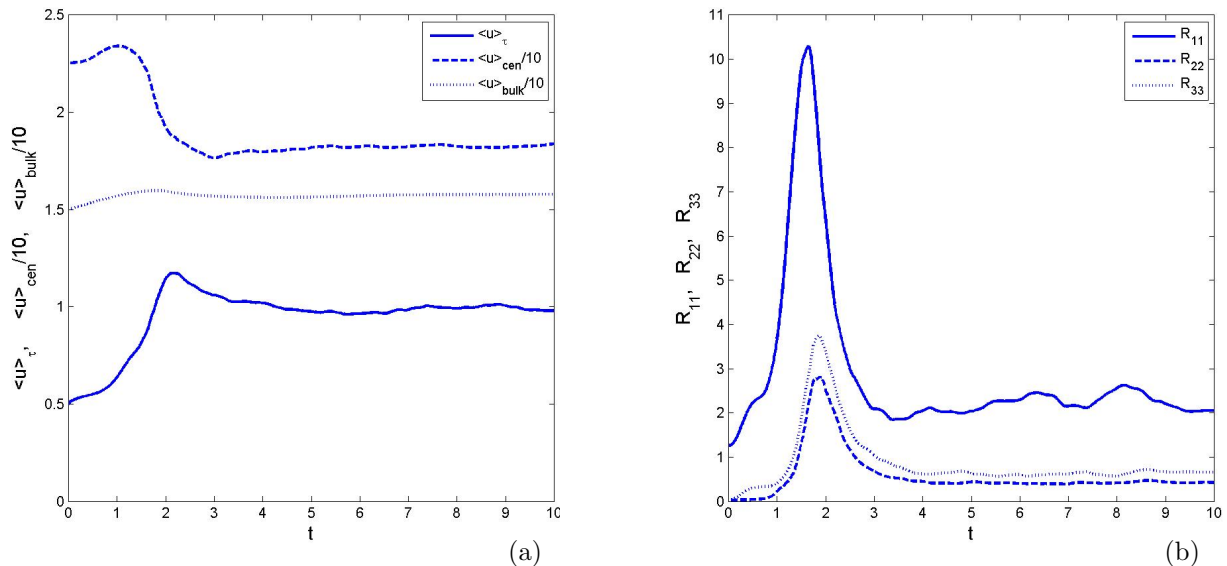


Figure 2: Time-dependent behaviour of spatially averaged quantities for simulation A1; (a): $\langle u \rangle_\tau$ (solid), $\langle u \rangle$ at the centerline divided by 10 (dashed), and bulk value $\int \langle u \rangle dy / L_y$ divided by 10 (dotted); (b) R_{ii} for $i = 1$ (solid), 2 (dashed), 3 (dotted).

zero if the grid size converges to zero. The derived boundary condition for ϕ is also different from that of the pressure. The boundary condition is $G_y \phi = 0$ on the walls, which is implied by the requirement $\tilde{v}^0 = v^0$ on the walls.

Table 2 shows an overview of the performed simulations. The simulations A1-4 and A3R were performed with the projection method described in section 2, which is a discretization of system NS. For simulations B1-4 the same method was used, except that the pressure at the new time level was defined as the pressure computed in the last stage of the time step. Simulations C1 and D1 were based on the discretization of two nonequivalent PPE systems, PPE1 and PPE3, respectively. All simulations were carried out in standard double precision (8-byte floating point). The grid stretching parameter γ was set to 1.4 in all cases. In all cases except A3R, the grid size in wall units was given by $h_{x+} = 8.8$, $h_{z+} = 5.9$, and $0.98 \leq h_{y+} \leq 4.5$. The center of the first grid cell adjacent to the wall was at $y_{c,1+} = 0.49$. These values were two times smaller in the case with the refined grid (A3R). The time step in simulation A1 was $\Delta t = 0.002$. In case A1 the (initial) maximum Courant number was about 1.0, while the maximum diffusion number equalled $4\nu\Delta t/h_{c,1}^2 \approx 1.5$, well within the stability region shown in Fig. 1.

The average over the spatially homogeneous directions $\langle \cdot \rangle$ is a function of y and t . It was implemented as a uniform average over all the grid points in xz -planes either at cell center location y_c or at staggered location y_s , dependent on the definition of the quantity averaged. The statistical mean, denoted by an overbar, is a function of y only, obtained by application of the average $\langle \cdot \rangle$ and subsequent averaging over time, based on samples between $t = 10$ and $t = 30$ (with a time interval of 0.1) from both sides of the channel (using the appropriate mirror condition with respect to the centerline). Temporal averaging over 20 time units was sufficient for the present purposes; tests with averaging over 90 time units in case A1 did not lead to noticeable differences on the scale of the present figures. The wall friction velocity was approximated by

$$\bar{u}_\tau = [(\bar{u}_1 - \bar{u}_0)/(y_{c,1} - y_{c,0})]^{1/2}, \quad (53)$$

where Eq. (20) was applied to the mean streamwise velocity \bar{u} . The numerical value of \bar{u}_τ after averaging over 20 time units was 1.000 and 0.999, for case A1 and A3R, respectively. Since $f_x = 1$ and total momentum is conserved the numerical value of \bar{u}_τ should converge to 1 in each case if the averaging time approaches infinity.

Figure 2 shows the temporal development of the flow, which undergoes a transition from the simple initial condition defined above to fully developed turbulent flow. Fig. 2a shows the quantity $\langle u \rangle_\tau = (\nu \partial \langle u \rangle / \partial y)^{1/2}$ evaluated at $y = 0$, which is a friction velocity that depends on time; it is initially 0.5, it increases and attains a value above 1.0 around $t = 2$, and afterwards it decreases and fluctuates around

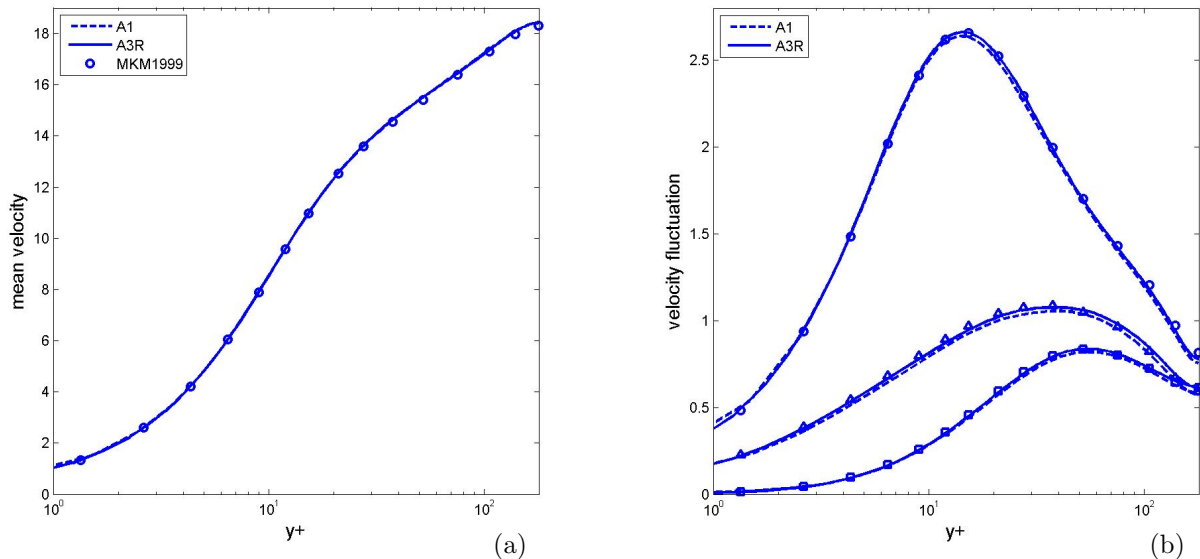


Figure 3: (a) Mean flow \bar{u} and (b) velocity fluctuations $(\overline{u_i^2} - \bar{u}_i^2)^{1/2}$ for x -direction $i=1$ (circles), y -direction $i=2$ (squares), and z -direction $i=3$ (triangles). Simulation A1 (dashed), A3R (solid), and Moser, Kim & Mansour [21] (symbols).

1.0, the statistical value of $u_\tau = \overline{\langle u \rangle}_\tau$. The center line and bulk values of $\langle u \rangle$ are also shown in Fig. 2a (divided by a factor 10). Fig. 2b shows the temporal development of the cross-sectionally averaged diagonal Reynolds stresses based on $\langle \cdot \rangle$, $R_{ii}(t) = \int (\langle u_i^2 \rangle - \langle u_i \rangle^2) dy / L_y$, where i denotes the spatial direction. These quantities peak around $t = 2$ and afterwards they saturate. For $t > 10$ fluctuations were similar to those shown between $t = 5$ and $t = 10$. For an integration in the normal direction the midpoint rule was used for quantities defined at y_c locations and the trapezoidal rule for quantities defined at y_s locations.

4.2. Numerical accuracy

Standard turbulence statistics of the simulations A1 and A3R are shown in Fig. 3 and compared with the data reported in Ref. [21]. The effect of the combined spatial and temporal truncation error is illustrated by the difference between cases A1 and A3R for a given statistical quantity. Since the method is second-order and the grid ratio equals 2 in each direction, estimates based on the Taylor expansion show that the truncation error in A3R is about 1/3 of the difference between A1 and A3R, and that the truncation error in A1 is about 4/3 times the difference. This and later comparisons between A1 and A3R confirm that the accuracy of A3R is good and the accuracy of A1 sufficient for the present purposes.

Figure 4 shows the evolution of the root of the average pressure variance $R_{pp}(t) = \int (\langle p^2 \rangle - \langle p \rangle^2) dy / L_y$ for different cases. Here the spatial and temporal truncation errors in the various cases cause visible differences after $t \approx 1.5$, and these differences show apparently chaotic behaviour after $t > 3$, due to the developed turbulence. The curves of simulations A1 and D1, which have the same truncation errors, but different round-off errors, are on top of each other until much later time (until $t \approx 7$). Since round-off errors are much smaller than truncation errors, physical instabilities triggered by the round-off errors take more time to grow to a significant level.

The energy produced by the convective scheme (integral of innerproduct of convective term and \mathbf{u}) was verified to be zero to machine precision at all times. Although the viscous scheme could not be proven to be formally negative-definite, no stability problems were encountered (except in case C1, discussed in section 5.4). The robustness of the present method was further tested by coarsening the grid of case A1. Simulations were performed on all grids $2^{k+1} \times 2^k \times 2^k$ with $1 \leq k \leq 7$ and k an integer value. All these simulations were numerically stable. In another test the physical viscosity was set to zero, and also that simulation was stable.

We finish this subsection with a verification of the order of the Runge-Kutta method. Usually the temporal order of numerical methods is shown for relatively simple test cases solved over a short time. We

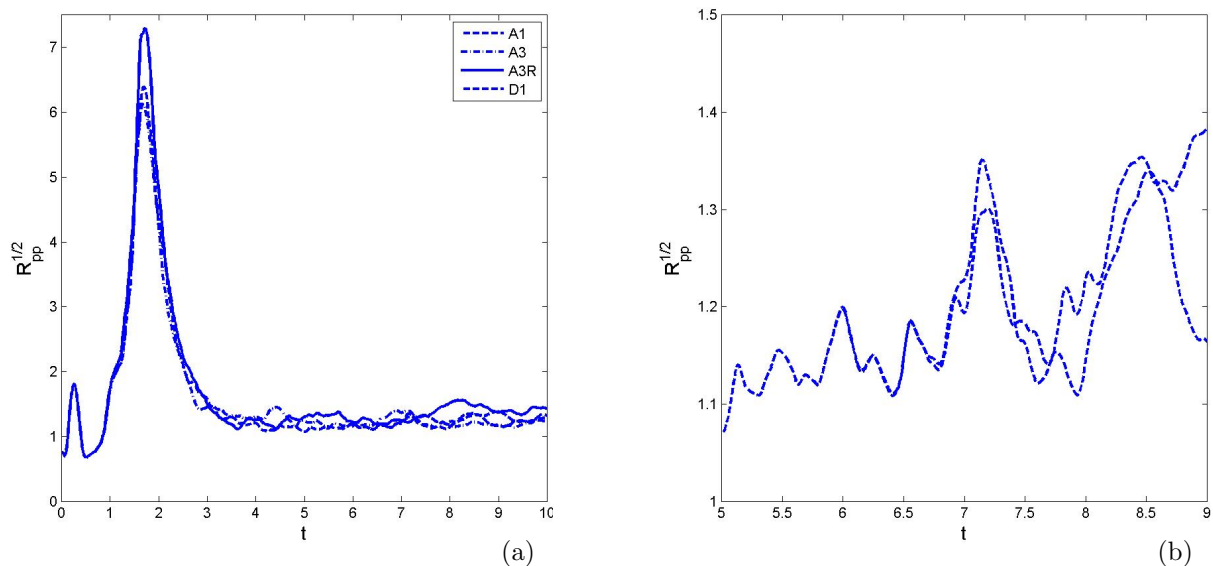


Figure 4: Average pressure fluctuation $R_{pp}^{1/2}$. Simulation A1 (dashed), A3 (dash-dotted), A3R (solid), and D1 (dotted). The second plot shows that the curves of A1 and D1 coincide until $t = 7$.

will investigate to which extent we can verify the order of temporal accuracy of a case that undergoes a transition to fully developed turbulent flow. For this purpose we performed simulations A1-4, performed with time step reduction of a factor 2 in consecutive cases. In simulations A1-4 (and A1S, A3R, C1) the pressure at the end of a time step (t^{n+1}) is identified with the pressure obtained in the first stage of the next time step $t^{n+1,0}$. However, simulations B1-4 were performed with the usual approach, the identification of the pressure at time t^{n+1} with the pressure computed in the last stage of the time step $t^{n,2}$. For a quantity q computed in three simulations with time steps Δt , $\Delta t/2$ and $\Delta t/4$, resulting in q_1 , q_2 and q_3 respectively, we define an approximation of the order of accuracy by

$$Q = \text{sign}[(q_1 - q_2)/(q_2 - q_3)] \times 2 \log |(q_1 - q_2)/(q_2 - q_3)|. \quad (54)$$

If the truncation error of q is proportional to $(\Delta t)^\beta$, then Q equals β . Figure 5 shows Q for 2 quantities and 4 triplets of simulations, (A1, A2, A3), (A2, A3, A4), (B1, B2, B3) and (B2, B3, B4).

Fig. 5a shows Q obtained for the quantity $q(t) = \langle u \rangle_\tau(t)$. Since the simulations only differ with respect to the interpretation of the pressure, results of series A and B coincide in Fig. 5a. For very short times $Q \approx 3$. Around $t = 0.1$ we see negative Q for a very short time. Negative or very large values often indicate the change of the ordering $q_1 < q_2 < q_3 < q_4$ to the ordering $q_1 > q_2 > q_3 > q_4$, or vice-versa. This was also the case at $t = 0.1$. For $t > 0.1$ the order of the method appears to be around 2. For $t > 1$ the behaviour of Q shows more noise, probably because temporal and spatial truncation errors start to interfere when the flow becomes turbulent. For this reason Q is not shown for $t > 2$.

Fig. 5b shows Q obtained for a quantity based on the pressure, $q(t) = R_{pp}(t)$. It clearly indicates that the temporal order of accuracy of series A is higher than of series B. The value $Q(R_{pp})$ for series A is about 3 for $t < 0.1$, almost 2 for $t < 0.35$, then increases to a higher value again. The conclusion is that the pressure in the present projection method is indeed second-order accurate in time. However, the results for series B in Fig. 5b ($Q(R_{pp}) \approx 1$) show that the conventional method, in which the pressure at the new time level is identified with the pressure computed in the last stage of the time step, is only first-order accurate, see also Ref. [14].

In the simulations presented in this paper the velocity on Γ did not depend on time. However, short-time simulations of cases A1-4 modified for time-dependent velocity on the walls were also performed. For a time dependent tangential velocity component on the walls, the temporal accuracy of the pressure remained second-order. However, for a time-dependent normal velocity component on the walls, the pressure was found to be only first-order accurate in time. If the normal component of the velocity on a Dirichlet boundary condition is time dependent and the continuity equation is rewritten as an equation

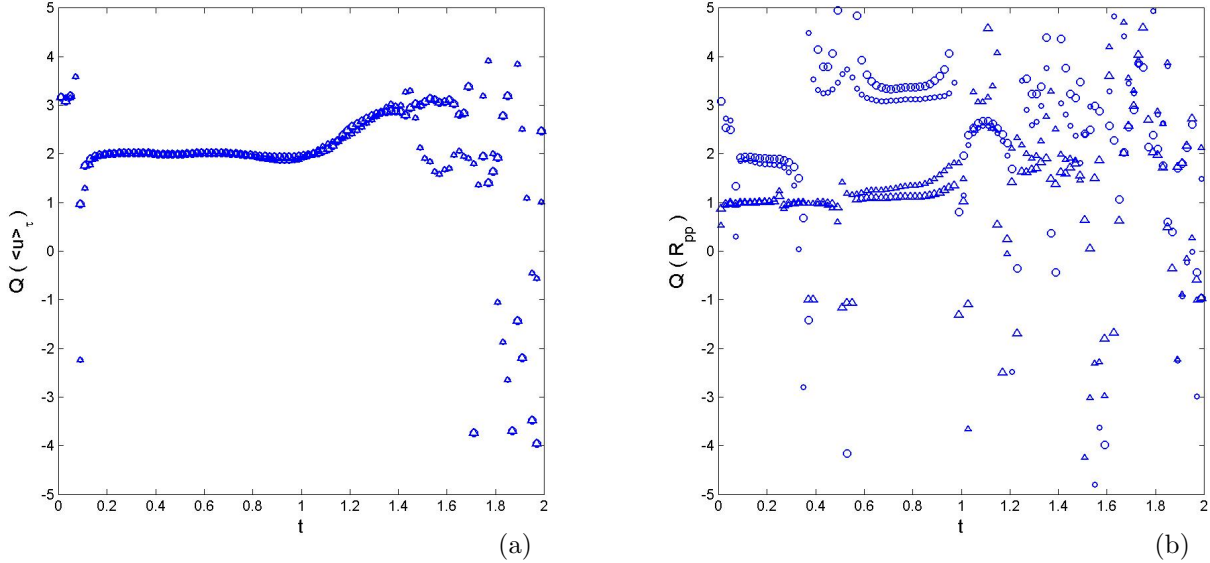


Figure 5: Convergence ratios $Q(\langle u \rangle_\tau)$ (a) and $Q(R_{pp})$ (b) for simulation triple (A1, A2, A3) (small circles), (A2, A3, A4) (large circles), (B1, B2, B3) (small triangles), (B2, B3, B4) (large triangles).

with unknowns at the left- and known quantities on the right-hand side, then the right-hand side depends on time and this usually leads to reduction of the temporal order of the pressure, see Ref. [14] and the discussion on differential algebraic equations in Ref. [7], section 3.16.

5. The pressure gradient near the wall

5.1. Comparison of NS, PPE1 and PPE3

In this subsection results are presented for the discrete PPE1 and PPE3 systems and compared with results of system NS. PPE1 and PPE3 have been implemented (a) to show, by comparison with PPE1, that the PPE3 condition of zero divergence of the velocity Laplacian near the wall is essential, (b) to verify the discrete equivalence between PPE3 and the projection method proven in section 3, (c) to show that the effect of the accumulation of precision errors on the divergence in PPE systems that use an exact solver for the Poisson equation is negligible, and (d) to compute the physical value of $\partial p / \partial y$ on the wall, which naturally appears in PPE3. It is remarked that the outcome of (c) is not evident, since in contrast to the projection method, zero divergence of the velocity in a PPE system relies on the induction principle, as explained in section 3. To know the physical wall value of $\partial p / \partial y$ can be important in applications, for example if the solution is used to track the motion of Lagrangian particles that depend on the pressure gradient force, which requires accurate interpolation of the pressure gradient at any particle location. However, the purpose of the present implementation of PPE3 is to illustrate the theory in section 3 and certainly not to provide a practical alternative for the more convenient projection method. If desired, the latter can be extended with a computation of the physical wall value of $\partial p / \partial y$ provided by PPE3 (see section 3.3).

The equivalence of the discrete versions of PPE3 and the projection method is demonstrated by Fig. 4b, where the curves of D1 and A1 coincide up to $t = 7$, and by Fig. 6a, which shows that the absolute velocity divergence remained below 10^{-8} in case D1 for an extended simulation time (until $t = 100$). Since the flow is turbulent, equivalent methods do not necessarily show the same time dependence. Indeed, Fig. 4b shows visible deviations between A1 (projection method) and D1 (PPE3), but only after $t = 7$, when the flow has been turbulent for some time.

The catastrophic growth of the divergence in simulation C1 (Fig. 6a, logarithmic scaling of both axes) demonstrates that the near-wall condition of zero divergence of the velocity Laplacian, which is missing in PPE1, is a crucial feature of PPE3. Comparison of cases D1 and A1 in Fig. 6a shows that the accumulation of divergence round-off errors in case D1 remained negligible.

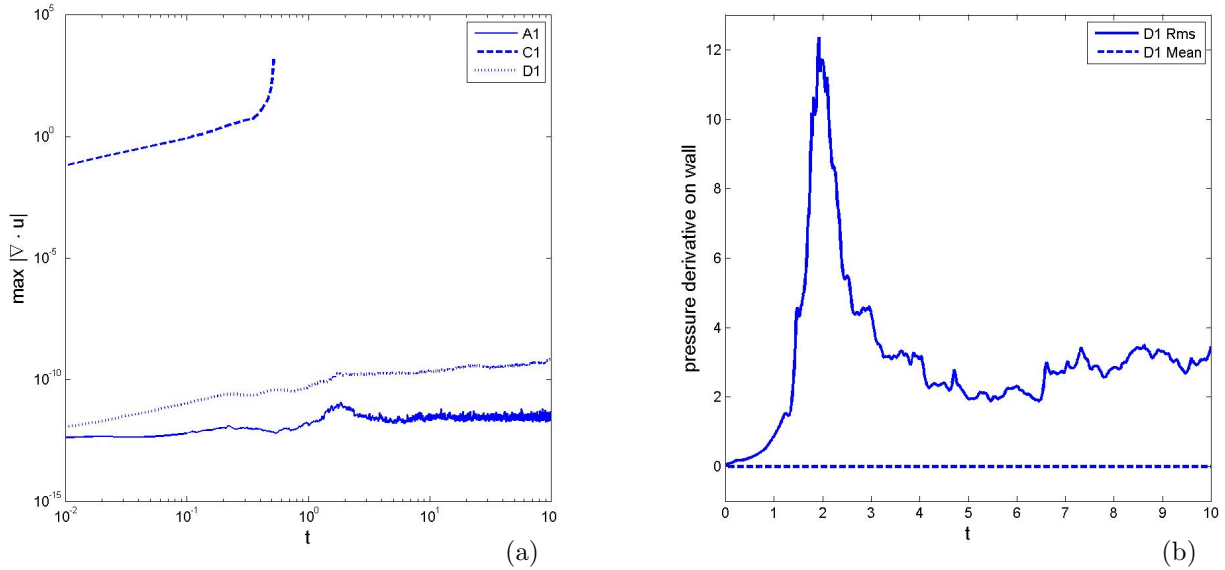


Figure 6: (a) Maximum $|\nabla \cdot \mathbf{u}|$ as function of time for simulation A1 (projection method, solid) and C1 (PPE1, dashed) and D1 (PPE3, dotted). (b) Normal component of the pressure gradient on the walls for simulation D1: $\langle (\partial p / \partial y)^2 \rangle - (\partial p / \partial y)^2$ (solid) and $\langle \partial p / \partial y \rangle$ (dashed).

The no-slip condition $\mathbf{u} = 0$ on Γ implies $-\mathbf{u} \cdot \nabla \mathbf{u} = \partial \mathbf{u} / \partial t = \mathbf{0}$ on Γ . Thus convective and time derivatives in the definition of the Neumann pressure boundary condition vanish. In addition $f_y = 0$ in this case, such that the wall boundary condition for the pressure Poisson equation in PPE3 reduces to

$$\partial p / \partial y = \nu \nabla^2 v \quad \text{on } \Gamma. \quad (55)$$

Fig. 6b shows the average and rms of the physical value of $\partial p / \partial y$ on the walls, defined with respect to the operator $\langle \cdot \rangle$ (on the walls an average over the periodic directions and the two walls). The rms value is nonzero, but the average is zero. The latter is consistent with the averaged Navier-Stokes equations for this case, since the continuity equation implies $\langle v \rangle = 0$ in the entire domain, and therefore Eq. (55) implies $\langle \partial p / \partial y \rangle = 0$ on the wall.

5.2. Short-time near-wall behaviour

In this subsection the discontinuity of the velocity acceleration at $t = 0$ is considered in more detail for the channel flow case. Each component of the velocity acceleration vector consists out of 3 non-trivial contributions, convective ($-\mathbf{u} \cdot \nabla \mathbf{u}$), pressure gradient ($-\nabla p$), and viscous term ($\nu \nabla^2 \mathbf{u}$). The fourth contribution is the trivial force term \mathbf{f} , which is 1 for the streamwise component and 0 for the other components.

Profiles of the magnitude of the three components of the convective term at $t = 0$, $t = 0.004$ and $t = 0.02$ are shown in Fig. 7a. The time-dependent magnitude of a quantity c is defined by $\langle c^2 \rangle^{1/2}$, which is a function of y and t . Due to the no-slip condition and the multiplication with \mathbf{u} in the definition of the convective terms, the magnitude of the convective term tends to zero if the wall is approached. The magnitude of the pressure gradient vector, shown in Fig. 7b, does not tend to zero for $y \rightarrow 0$, but it appears to be smooth in space and also in time, since the profiles for the three distinct times are close to each other.

Profiles of the three components of the viscous term are shown in Fig. 8. In contrast to Fig. 7, we do see a strong effect within a few time steps, but only for the tangential components (note that the scale on the vertical axis in Fig. 8b was divided by 10). We define the wall values of these quantities as the limits from the interior, also for $t = 0$, since the initial velocity is a smooth function of \mathbf{x} by definition. Thus we can conclude from Fig. 8 that, on the wall, the Laplacians of the streamwise and spanwise velocity components are discontinuous functions of time at $t = 0$. In contrast to the Laplacians of the tangential velocities, the Laplacian of the normal component does not display discontinuous behaviour.

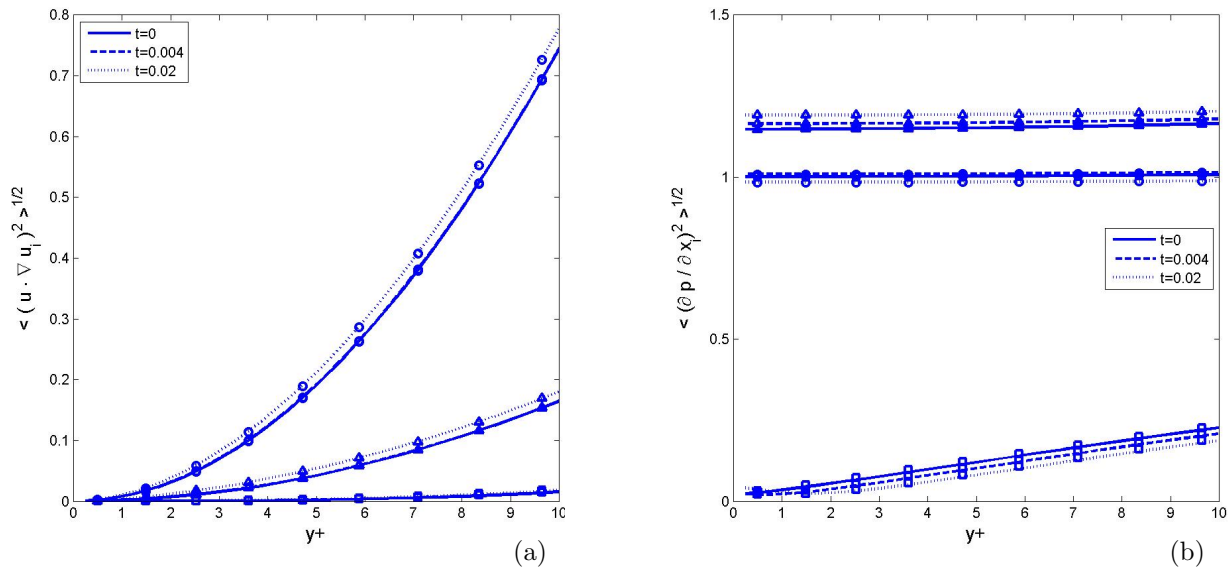


Figure 7: Short-time behaviour of (a) convective terms $\langle (\mathbf{u} \cdot \nabla u_i)^2 \rangle^{1/2}$, and (b) pressure terms $\langle (\partial p / \partial x_i)^2 \rangle^{1/2}$, for stream-wise component $i = 1$ (circles), normal component $i = 2$ (squares), spanwise component $i = 3$ (triangles). Profiles are shown for $t = 0$ (solid), $t = 0.004$ (dashed) and $t = 0.02$ (dotted). Simulation A1 (symbols) and simulation A3R (lines).

The total acceleration of the three velocity components is shown in Fig. 9. The behaviour is consistent with Figs. 7-8. Since by definition $\partial \mathbf{u} / \partial t$ is zero on the wall, the tangential components appear to be discontinuous functions of y at $y = 0$ and $t = 0$. It is not possible to extend $\partial u / \partial t$ (nor $\partial w / \partial t$) to a continuous function in space and time; the space-time limit approaching a point on the wall at $t = 0$ does in general not exist, because according to Fig. 9 the limit at $t = 0$ ($y \rightarrow 0$) differs from the limit at $y = 0$ ($t \rightarrow 0$), which is zero by definition. However, for $t > 0$ the discontinuous profiles have evolved into a smooth profiles by viscous diffusion. The discontinuous behaviour at $t = 0$ is caused by the fact that no pressure can be obtained that satisfies the momentum equation on the wall in all three directions at $t = 0$, not for the present initial condition, nor for any other initial condition that can easily be expressed into simple analytical functions. However, the normal velocity acceleration appears to be continuous on the wall at $t = 0$. That continuity is observed in the normal direction, but not in the tangential ones, shows that the solution still satisfies the normal momentum equation if not all three momentum equations can be satisfied on the wall. This confirms that in case a component of the momentum equation is used to derive a pressure boundary condition for Poisson equation (4), this should be the normal component and not one of the tangential components, see Refs. [5, 7, 16].

5.3. The near-wall limit in the turbulent regime

The statistical near-wall behaviour of the pressure gradient and the sum of pressure and viscous terms in the turbulent regime is shown in Fig. 10. Results are shown for simulation A1 and the refined simulation A3R. The magnitude of each component of the pressure term (pressure gradient) appears to converges to a nonzero value on the wall. The magnitude of the sum of the pressure, viscous and force term converges to zero on the wall, for each component. This indicates that in each direction the nonzero pressure gradient is balanced by a nonzero viscous plus force term on the wall. In addition it was verified that the magnitude of the convective term approaches zero in the near-wall limit. Therefore, Fig. 10b indicates that in the turbulent regime $\partial \mathbf{u} / \partial t$ is continuous in the near-wall limit. In other words, in the turbulent regime each component of the momentum equation is satisfied on the wall.

5.4. H1980 and HR1982

The results shown in the previous two subsections indicate that the computed velocity satisfies the regularity of the solution described in H1980 (see Introduction). First, the velocity appears to be smooth for $0 < t < T$ in the interior of the domain (Ω). Second, the velocity is continuous at $t = 0$ and on Γ .

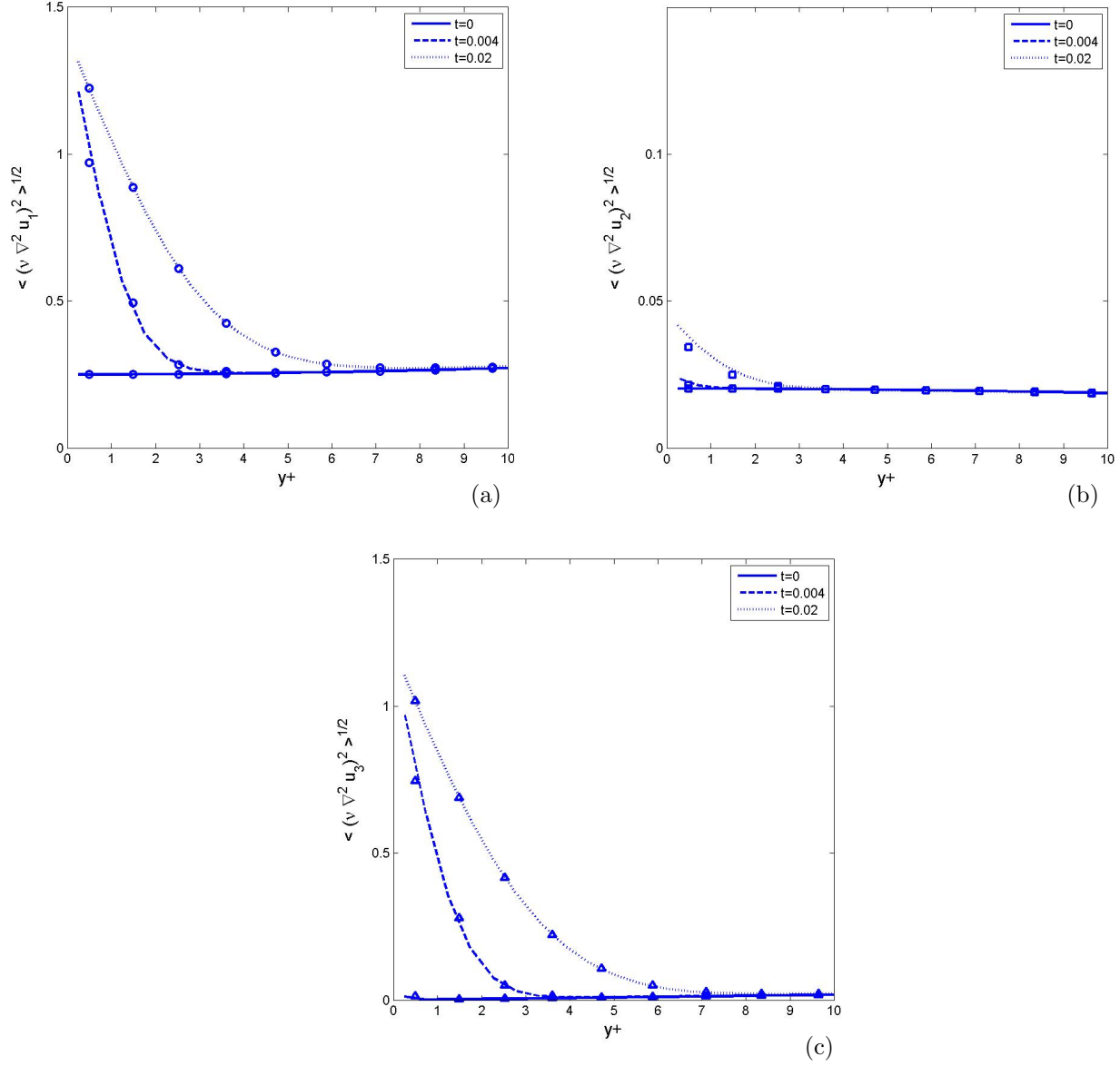


Figure 8: Short-time behaviour of viscous terms $\langle (\nu \nabla^2 u_i)^2 \rangle^{1/2}$ for (a) $i = 1$, (b) $i = 2$, and (c) $i = 3$. Profiles are shown for $t = 0$ (solid), $t = 0.004$ (dashed) and $t = 0.02$ (dotted). Note that the vertical scale in (b) is 10 times smaller than in (a) and (c). Simulation A1 (symbols) and simulation A3R (lines).

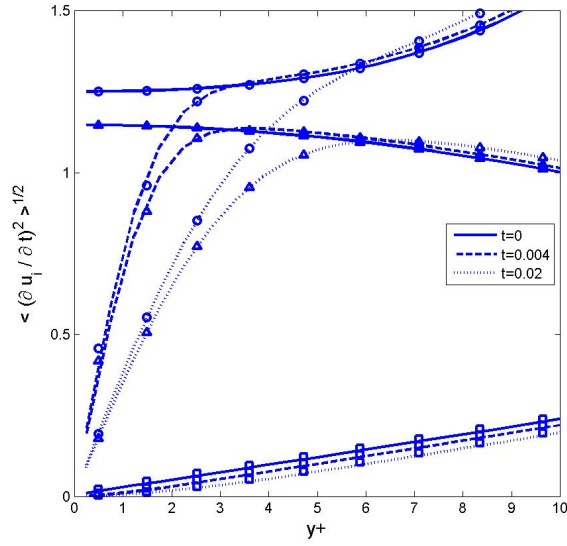


Figure 9: Short-time behaviour of acceleration terms $\langle (\partial u_i / \partial t)^2 \rangle^{1/2}$ for $i = 1$ (circles), 2 (squares), 3 (triangles). Profiles are shown for $t = 0$ (solid), $t = 0.004$ (dashed) and $t = 0.02$ (dotted). Simulation A1 (symbols) and simulation A3R (lines).

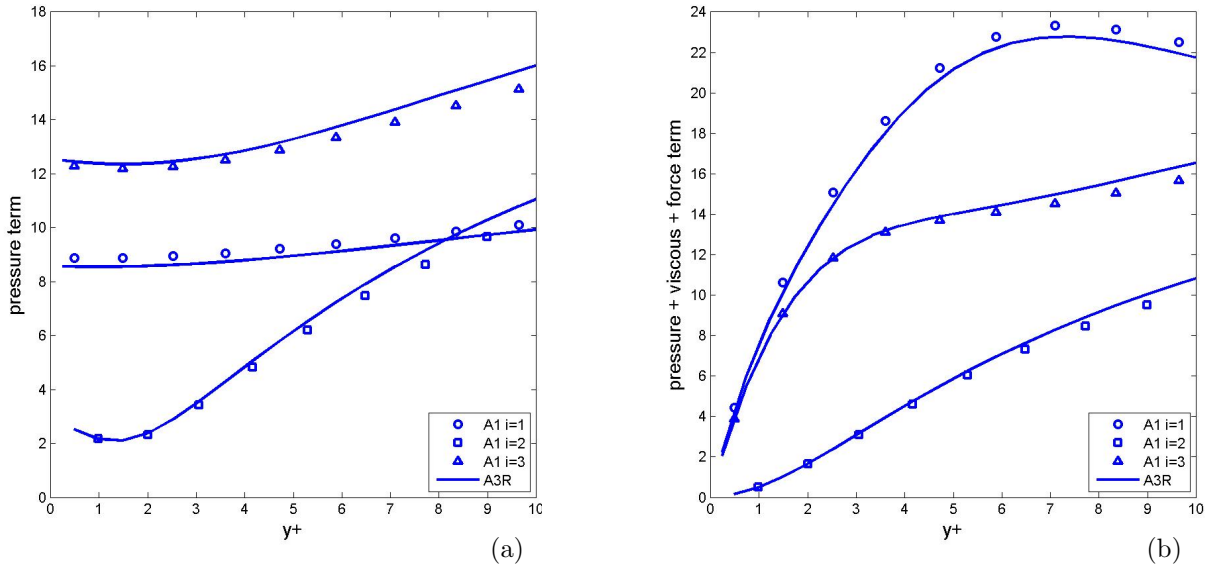


Figure 10: Near-wall behaviour in turbulent regime, magnitudes $(\overline{q_i^2})^{1/2}$ for (a) $q_i = -\partial p / \partial x_i$, and (b) $q_i = -\partial p / \partial x_i + \nu \nabla^2 u_i + f_i$. Simulation A1 (symbols) and A3R (solid). Streamwise direction $i=1$ (circles), normal direction $i=2$ (squares) and spanwise direction $i=3$ (triangles).

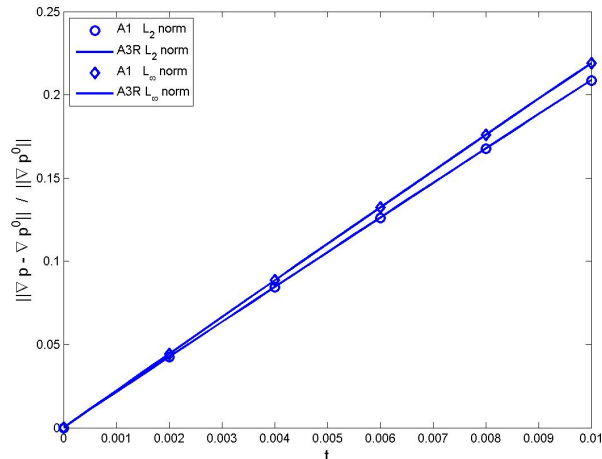


Figure 11: Short time behaviour of $\|\nabla p - \nabla p^0\|_2 / \|\nabla p^0\|_2$ (solid) and $\|\nabla p - \nabla p^0\|_\infty / \|\nabla p^0\|_\infty$ (dotted). Symbols are from simulation A1, lines are from simulation A3R.

Non-smoothness is also observed; the tangential components of $\partial \mathbf{u} / \partial t$ are discontinuous in space and time on Γ at $t = 0$.

In fact, the numerical solution seems to obey even stronger regularity than described in H1980: (a) The normal component of the time derivative and all components of the pressure gradient look smooth, both in space and time on $[0, T) \times \bar{\Omega}$, which includes both $t = 0$ and Γ ; (b) All quantities, including the tangential components of $\partial \mathbf{u} / \partial t$, seem to be smooth in time at $t = 0$ in the interior of the domain; time discontinuity occurs only on the walls; (c) The velocity and pressure display spatial smoothness for $0 \leq t < T$, also on Γ .

As an illustration of HR1982 (see Introduction), we consider the convergence of the pressure in the limit of $t \rightarrow 0$ in more detail. Figure 11 shows the behaviour of the L_2 -norm and L_∞ -norm of $\nabla p - \nabla p^0$ for small times. Both norms tend to zero if $t \rightarrow 0$. This result supports HR1982, but does not support Lemma 3 in Ref. [8]. In fact, HR1982 claimed convergence in the L_2 -norm, while the numerical result suggests stronger convergence, in L_2 and in L_∞ . Like results in previous subsections, this result was validated by grid refinement; Fig. 11 shows very similar curves for simulation A1 and refined simulation A3R. The L_2 -norm of a vector $\mathbf{g} = (g_x, g_y, g_z)$ that is discretely available at staggered locations is an approximation of $(\int g_x^2 d\mathbf{x} + \int g_y^2 d\mathbf{x} + \int g_z^2 d\mathbf{x})^{1/2}$, where the first and third integral are approximated with midpoint and the second integral with trapezoidal integration over the domain.

In HR1982, p^0 is defined as the solution of the pressure Poisson equation at $t = 0$ with a boundary condition for the normal component of the pressure gradient. It is also possible to solve the pressure Poisson equation at $t = 0$ with a tangential component of the pressure gradient prescribed on Γ . Say that q^0 is the solution for a tangential boundary condition. A numerical example in Ref. [8] shows that in general $q^0 \neq p^0$. Then the logical consequence of HR1982 can only be that in general ∇p does not converge to ∇q^0 if $t \rightarrow 0$.

6. Conclusions

We considered an explicit projection method for the incompressible Navier-Stokes equations with no-slip walls, discretized on a staggered grid. The method was analyzed and used in simulations to address several issues related to the formulation of the wall boundary condition for the standard pressure Poisson equation (PPE), $\nabla^2 p = \nabla \cdot (-\mathbf{u} \cdot \nabla \mathbf{u} + \mathbf{f})$. Three research questions were formulated in the Introduction and the answers to these questions are presented below.

The first question was whether the standard pressure Poisson equation with Neumann boundary derived from the normal component of the momentum equation, $\partial p / \partial n = \mathbf{n} \cdot (\nu \nabla^2 \mathbf{u} + \mathbf{f} - \mathbf{u} \cdot \nabla \mathbf{u} - \partial \mathbf{u} / \partial t)$, could be made consistent with the Navier-Stokes equations. It was shown that if the requirement that

$\nabla \cdot \nabla^2 \mathbf{u} = 0$ is zero near the wall is added to the system, the PPE problem is equivalent to the Navier-Stokes equations for sufficiently smooth solutions, without the need to introduce Green's functions. This PPE system was called PPE3.

The second research question was which continuous PPE system is in discrete form equivalent to the staggered projection method. An answer would clarify the relation between PPE systems on the one hand and the staggered projection method on the other hand. Such a clarification was desirable since the term pressure Poisson equation is often used to describe the pressure equation solved in the staggered projection method. Two discrete PPE systems were found to be equivalent to the staggered projection method: above mentioned PPE3 and a system which uses a seemingly vanishing viscous term on the right-hand side (PPE2). Thus PPE3 had several theoretical purposes. Apart from providing an answer to the first research question, PPE3 turned out to be useful to clarify the relation between the projection method and PPE systems, to clarify the so-called PPE paradox by a discrete analysis, and to derive the physical wall value of $\partial p / \partial n$ implied (not required) by the projection method.

The third research question was about the near-wall behaviour of a solution of the Navier-Stokes equations, for all t , but in particular for $t \rightarrow 0$. This topic was considered because the Neumann condition for the PPE can only be valid in combination with appropriate regularity of the solution of the Navier-Stokes equations near and on the wall. Direct Numerical Simulation of turbulent channel flow at $Re_\tau=180$ was performed, starting from a precisely prescribed smooth initial condition. The staggered projection method, which is known to be equivalent to a direct discretization of the Navier-Stokes equation (no pressure boundary condition), was used in the simulation. Numerical inspection of the separate terms of the momentum equation in the near-wall region indicated that the three components of the momentum equation were valid on the wall for $t > 0$ (verified for short times and in the fully developed turbulent regime). In the limit $t \rightarrow 0$, the pressure gradient appeared to converge to the initial pressure gradient in the L_2 -norm, which confirmed a disputed theoretical result in literature. The numerical results also indicated stronger regularity than claimed by existing theorems. Even in the maximum norm, the pressure gradient appeared to converge to the initial pressure gradient. In fact the only discontinuities observed in the simulations were discontinuities of the tangential viscous terms and the time derivatives of the tangential velocities on the wall at $t = 0$.

Acknowledgement

An example of an initial perturbation for turbulent channel flow, similar to the one used in this paper, was kindly provided by N.D. Sandham. The author is grateful to J.G.M. Kuerten for interesting discussions about numerical methods and to the Reviewers for useful comments.

Appendix 1: Extrapolation coefficients

The coefficients of the fourth-order extrapolation Eq. (21) are specified here. For brevity the center grid locations $y_{c,j}$ are denoted by y_j . For a wall located at $y = 0$, the coefficients are

$$\beta_1 = (s_{11}y_0 + s_{12}y_0^2 + s_{13}y_0^3)/s, \quad (56)$$

$$\beta_2 = (s_{21}y_0 + s_{22}y_0^2 + s_{23}y_0^3)/s, \quad (57)$$

$$\beta_3 = (s_{31}y_0 + s_{32}y_0^2 + s_{33}y_0^3)/s, \quad (58)$$

where s_{ij} is given by the matrix

$$\begin{pmatrix} y_2^2 y_3^2 (y_3 - y_2) & y_2 y_3 (y_2^2 - y_3^2) & y_2 y_3 (y_3 - y_2) \\ y_3^2 y_1^2 (y_1 - y_3) & y_3 y_1 (y_3^2 - y_1^2) & y_3 y_1 (y_1 - y_3) \\ y_1^2 y_2^2 (y_2 - y_1) & y_1 y_2 (y_1^2 - y_2^2) & y_1 y_2 (y_2 - y_1) \end{pmatrix}, \quad (59)$$

and

$$s = y_1 y_2 y_3 (y_2 y_3 (y_3 - y_2) + y_3 y_1 (y_1 - y_3) + y_1 y_2 (y_2 - y_1)). \quad (60)$$

For completeness coefficients for lower order extrapolations are also provided:

$$\beta_1 = \frac{y_0(y_2 - y_0)}{y_1(y_2 - y_1)}, \quad \beta_2 = \frac{y_0(y_1 - y_0)}{y_2(y_1 - y_2)}, \quad \beta_3 = 0, \quad (61)$$

for a third-order extrapolation, and $\beta_1 = -y_0/(y_1 - y_0)$, $\beta_2 = \beta_3 = 0$, for a second-order extrapolation. For the example given in Table 1, this second-order extrapolation with y_0 given by Eq. (14) produces the same results as Eq. (21).

Appendix 2: Proof of statement (46)

In this appendix we prove (46), which states that $\mathbf{D} \cdot \mathbf{b}^{n,m} = 0$ for $2 \leq j \leq N - 1$ if $\mathbf{D} \cdot \mathbf{u}^{n,m} = 0$ for $1 \leq j \leq N$. For brevity, we omit the superscripts m, n and write the components of \mathbf{b} as

$$b_x = \nu B_u u, \quad b_y = \nu B_v v, \quad b_z = \nu B_w w, \quad (62)$$

where B_u , B_v and B_w refer to the discrete Laplace operator at staggered u -locations, v -locations and w -locations, respectively, for example $B_u = B_{u,x} + B_{u,y} + B_{u,z}$. In addition we define a discrete Laplace operator on center locations, $B_c = B_{c,x} + B_{c,y} + B_{c,z}$. On Cartesian grids, the following is true for cell centers that are not adjacent to the wall ($2 \leq j \leq N - 1$):

$$\begin{aligned} \mathbf{D} \cdot \mathbf{b} &= D_x B_{u,x} u + D_x B_{u,y} u + D_x B_{u,z} u + \\ &\quad D_y B_{v,x} v + D_y B_{v,y} v + D_y B_{v,z} v + \\ &\quad D_z B_{w,x} w + D_z B_{w,y} w + D_z B_{w,z} w \\ &= B_{c,x} D_x u + B_{c,y} D_x u + B_{c,z} D_x u + \\ &\quad B_{c,x} D_y v + B_{c,y} D_y v + B_{c,z} D_y v + \\ &\quad B_{c,x} D_z w + B_{c,y} D_z w + B_{c,z} D_z w \\ &= B_c (\mathbf{D} \cdot \mathbf{u}). \end{aligned} \quad (63)$$

The nontrivial part here are the nine 'commutations', for example

$$D_y B_{v,y} v = B_{c,y} D_y v, \quad (64)$$

which is not really a commutation, since the operator $B_{v,y}$ is not precisely the same as $B_{c,y}$. To show the validity of (64), we write

$$\begin{aligned} D_y B_{v,y} v &= \frac{1}{h_{c,j}} \left[\frac{1}{h_{s,j}} \left(\frac{v_{j+1} - v_j}{h_{c,j+1}} - \frac{v_j - v_{j-1}}{h_{c,j}} \right) - \frac{1}{h_{s,j-1}} \left(\frac{v_j - v_{j-1}}{h_{c,j}} - \frac{v_{j-1} - v_{j-2}}{h_{c,j-1}} \right) \right] \\ &= \frac{1}{h_{c,j}} \left[\frac{1}{h_{s,j}} \left((D_y v)_{j+1} - (D_y v)_j \right) - \frac{1}{h_{s,j-1}} \left((D_y v)_j - (D_y v)_{j-1} \right) \right] \\ &= B_{c,y} D_y v. \end{aligned} \quad (65)$$

Similarly, one can derive $D_x B_{u,x} = B_{c,x} D_x$, $D_x B_{u,y} = B_{c,y} D_y$, etc. If $\mathbf{D} \cdot \mathbf{u} = 0$ for $1 \leq j \leq N$, Eq. (63) implies that $\mathbf{D} \cdot \mathbf{b} = 0$ for $2 \leq j \leq N - 1$.

References

- [1] P. Moin and J. Kim, On the numerical solution of time-dependent viscous incompressible fluid flows involving solid boundaries, *J. Comput. Phys.* 35 (1980) 381-392.
- [2] L. Kleiser and U. Schumann, Treatment of Incompressibility and Boundary Conditions in 3-D Numerical Spectral Simulations of Plane Channel Flows, in: E.H. Hirschel (ed.), *Proc. 3rd GAMM Conf. on Numerical Methods in Fluid Mechanics*, Vieweg-Verlag, Braunschweig, 1980, pp. 165-173.
- [3] R. Peyret and T.D. Taylor, *Computational methods for fluid flow*, Springer-Verlag, New York, 1983.
- [4] S.A. Orszag, M. Israeli and M.O. Deville, Boundary conditions for incompressible flows, *J. Sci. Comput.* 1 (1986) 75-111.
- [5] P.M. Gresho and R.L. Sani, On pressure boundary conditions for the incompressible Navier-Stokes equations, *Int. J. Numer. Methods Fluids* 7 (1987) 1111-1145.

- [6] A.E.P. Veldman, "Missing" boundary conditions? Discretize first, substitute next, combine later, *SIAM J. Sci. Stat. Comput.* 11 (1990) 82-91.
- [7] P.M. Gresho and R.L. Sani, *Incompressible flow and the finite element method*, John Wiley and Sons, Chichester, 1998.
- [8] D. Rempfer, On boundary conditions for incompressible Navier-Stokes problems, *Appl. Mech. Rev.* 59 (2006) 107-125.
- [9] R.L. Sani, J. Shen, O. Pironneau and P.M. Gresho, Pressure boundary condition for the time-dependent incompressible Navier-Stokes equations, *Int. J. Numer. Meth. Fluids* 50 (2006) 673-682.
- [10] F.E. Harlow and J.E. Welch, Numerical calculation of time-dependent viscous incompressible flow of fluid with free surface, *Phys. Fluids* 8 (1965) 2182.
- [11] A.J. Chorin, Numerical solution of the Navier-Stokes equations, *Math. Comput.* 22 (1968) 745-762.
- [12] R. Temam, Sur l'approximation de la Solution des équations de Navier-Stokes par la méthode des pas fractionnaires I, *Arch. Ration. Mech. Anal.* 32 (1969) pp. 135-153.
- [13] J.B. Perot, An Analysis of the Fractional Step Method, *J. Comput. Phys.* 108 (1993) 51-58.
- [14] B. Sandeher and B. Koren, Accuracy analysis of explicit Runge-Kutta methods applied to the incompressible Navier-Stokes equations, *J. Comput. Phys.* 231 (2012) 3041-3063.
- [15] J.G. Heywood, The Navier-Stokes equations: on the existence, regularity and decay of solutions, *Indiana Univ. Math. J.* 29 (1980) 639-680.
- [16] J.G. Heywood and R. Rannacher, Finite element approximation of the nonstationary Navier-Stokes problem. I. Regularity of solutions and second-order error estimates for spatial discretization, *SIAM Soc. Ind. Appl. Math. J. Numer. Anal.* 19 (1982) 275-311.
- [17] R. Temam, Behaviour at time $t=0$ of the solutions of semi-linear evolution equations, *J. Diff. Equ.* 43 (1982) 73-92.
- [18] P. Moin and J. Kim, Numerical investigation of turbulent channel flow, *J. Fluid Mech.* 118 (1982) 341-377.
- [19] J. Kim, P. Moin and R. Moser, Turbulence statistics in fully developed channel flow at low Reynolds number, *J. Fluid Mech.* 177 (1987) 133-166.
- [20] N.D. Sandham, Resolution requirements for Direct Numerical Simulation of near-wall turbulent flow using finite differences, Queen Mary and Westfield College Report QMW-EP-1097 (1994).
- [21] R.D. Moser, J. Kim, N.N. Mansour, Direct numerical simulations of turbulent channel flow up to $Re_\tau = 590$, *Phys. Fluids* 11 (1999) 943-945.
- [22] J.C. del Álamo and J. Jiménez, Spectra of the very large anisotropic scales in turbulent channels, *Phys. Fluids* 15 (2003) L41-43.
- [23] R.W.C.P. Verstappen, A.E.P. Veldman, Symmetry-preserving discretization of turbulent flow, *J. Comp. Physics* 187 (2003) 343-368.
- [24] H. Abe, H. Kawamura and Y. Matsuo, Surface heat-flux fluctuations in a turbulent channel flow up to $Re_\tau = 1020$ with $Pr = 0.025$ and $Pr = 0.71$, *Int. J. Heat and Fluid Flow* 25 (2004) 404-419.
- [25] Z.W. Hu, C.L. Morfey and N.D. Sandham, Wall pressure and shear stress spectra from direct numerical simulations of channel flow up to $Re_\tau = 1440$, *AIAA Journal* 44 (2006) 1541-1549.
- [26] J. Meyers and P. Sagaut, Is plane-channel flow a friendly case for the testing of large-eddy simulation subgrid-scale models? *Phys. fluids* 19 (2007) 048105.
- [27] J.C. Strikwerda and Y.S. Lee, The accuracy of the fractional step Method, *SIAM Soc. Ind. Appl. Math. J. Numer. Anal.* 37 (1999) 37-47.
- [28] S. Armfield and R. Street, The fractional-step method for the Navier-Stokes equations on staggered grids: the accuracy of three variations, *J. Comput. Phys.* 153 (1999) 660-665.

- [29] J. Kim and P. Moin, Application of a fractional-step method to incompressible Navier-Stokes equations, *J. Comput. Phys.* 59 (1985) 308- 323.
- [30] T.M. Burton and J.K. Eaton, Analysis of a fractional-step method on overset grids, *J. Comput. Phys.* 177 (2002) 336-364.
- [31] D.L. Brown, R. Cortez, and M.L. Minion, Accurate projection methods for the incompressible Navier-Stokes equations, *J. Comput Phys.* 168 (2001) 464-499.
- [32] N.D. Sandham and L. Kleiser, The late stages of transition in turbulent channel flow, *J. Fluid Mech.* 245 (1992) 319-348.
- [33] K. Akselvoll and P. Moin, An efficient method for temporal integration of the Navier-Stokes equations in confined axisymmetric geometries, *J. Comput. Phys.* 125 (1996) 454-463.
- [34] J.G.M. Kuerten, An accurate numerical method for DNS of turbulent pipe flow, in: V. Armenio, B. Geurts, J. Fröhlich (Eds.), *Direct and Large-Eddy Simulation VII*, ERCOFTAC Series Volume 13, 2010, pp. 131-136.
- [35] A. Jameson, Success and challenges in computational aerodynamics, *AIAA Paper*, No. 87-1184 (1987), 1-35.
- [36] A. Jameson, and T.J. Baker, Solution of the Euler equations for complex configurations, *AIAA Paper*, No. 83-1929 (1983), 293-302.
- [37] B. Vreman, B. Geurts and H. Kuerten, Large-eddy simulation of the turbulent mixing layer, *J. Fluid. Mech.* 339 (1997) 357-390.
- [38] A.W. Vreman, N.D. Sandham, K.H. Luo, Compressible mixing layer growth rate and turbulence characteristics, *J. Fluid. Mech.* 320 (1996) 235-258.
- [39] Y. Morinishi, T.S. Lund, O.V. Vasilyev and P. Moin, Fully conservative higher order finite difference schemes for incompressible flow. *J. Comput. Phys.* 143 (1998) 90-124.
- [40] P. Wesseling, *Principles of computational fluid dynamics*, Springer, Berlin, 2000.
- [41] G. Tryggvason and R. Scardovelli, *Direct numerical simulations of gas-liquid multiphase flows*, Cambridge University Press, Cambridge, 2011.
- [42] T.Y. Hou and B.R.R. Wetton, Second-order convergence of a projection scheme for the incompressible Navier-Stokes equations with boundaries, *Siam J. Numer. Anal.* 30 (1993), 609-629.
- [43] A.A. Amsden and F.H. Harlow, The SMAC method, Los Alamos Scientific Lab. Rep. No. LA-4370 (1970).
- [44] Q.H. Deng and G.F. Tang, Special treatment of pressure correction based on continuity conservation in a pressure-based algorithm, *Num. Heat Transfer, Part B.* 42 (2002) 73-92.